

# DYNAMICS NEAR A PERIODICALLY FORCED ROBUST HETEROCLINIC CYCLE

September 12, 2018

ISABEL S. LABOURIAU AND ALEXANDRE A. P. RODRIGUES  
CENTRO DE MATEMÁTICA DA UNIVERSIDADE DO PORTO AND  
FACULDADE DE CIÊNCIAS, UNIVERSIDADE DO PORTO

ABSTRACT. There are few examples of non-autonomous vector fields exhibiting complex dynamics that may be proven analytically. We analyse a family of periodic perturbations of a weakly attracting robust heteroclinic network defined on the two-sphere. We derive the first return map near the heteroclinic cycle for small amplitude of the perturbing term, and we reduce the analysis of the non-autonomous system to that of a two-dimensional map on a cylinder.

When the perturbation strength is small there is an attracting invariant closed curve not contractible on the cylinder. Near the centre of frequency locking there are parameter values for which this curve coexists with an attracting periodic solution. Increasing the perturbation strength there are periodic solutions that bifurcate into a closed contractible invariant curve and into a region where the dynamics is conjugate to a full shift on two symbols. These last two dynamical features appear at a discrete-time Bogdanov-Takens bifurcation.

**Keywords:** periodic forcing, heteroclinic cycle, global attractor, bifurcations, stability

**2010 — AMS Subject Classifications** Primary: 37C60; Secondary: 34C37, 34D20, 37C27, 39A23, 34C28

## 1. INTRODUCTION

Archetypal examples of robust heteroclinic cycles have been studied by Guckenheimer and Holmes [13], and May and Leonard [19], using a system of Lotka-Volterra equations. The authors found saddle-equilibria on the axes and attracting heteroclinic cycles and networks.

A heteroclinic cycle in an autonomous dynamical system consists of a connected union of saddle-type invariant sets and heteroclinic trajectories connecting them. A heteroclinic network is a connected union of heteroclinic cycles. In equivariant systems the existence of invariant subspaces may force the existence of connecting trajectories between flow-invariant sets; heteroclinic cycles become robust in the sense that the connections persist under small symmetry-preserving perturbations. In generic dynamical systems without symmetry or other constraints, such configurations are structurally unstable.

In classical mechanics, dissipative non-autonomous systems received only limited attention, in part because it was believed that, in these systems, all trajectories tend toward Lyapunov stable sets (fixed points or periodic solutions). Evidence that second order equations with a periodic forcing term can have interesting behavior first appeared in the study of van der Pol's equation, which describes an oscillator with nonlinear damping. Results of [8] pointed out an attracting set more complicated than a fixed point or an invariant curve. Levinson obtained detailed information for a simplified model [18].

---

Centro de Matemática da Universidade do Porto (CMUP — UID/MAT/00144/2013) is funded by FCT (Portugal) with national (MEC) and European structural funds through the programs FEDER, under the partnership agreement PT2020. A.A.P. Rodrigues acknowledges financial support from Program INVESTIGADOR FCT (IF/00107/2015). Part of this work has been written during AR stay in Nizhny Novgorod University partially supported by the grant RNF 14-41-00044.

Examples from the dissipative category include the equations of Lorenz, Duffing equation and Lorentz gases acted on by external forces [10]. The articles [9, 32] deal with heteroclinic tangles in time-periodic perturbations in the dissipative context and show, for a set of parameters with positive Lebesgue measure, the existence of an attracting torus, of infinitely many horseshoes and of strange attractors with SRB measures.

While some progress has been made, both numerically and analytically, the number of differential equations with periodic forcing whose flows exhibit attracting heteroclinic networks, for which a rigorous global description of the dynamics is available, has remained small. To date there has been very little systematic investigation of the effects of perturbations that are time-periodic, despite being natural for the modelling of many biological effects, see Rabinovich *et al* [24].

## 2. THE OBJECT OF STUDY

For  $\gamma, \omega \in \mathbf{R}_0^+$ , the focus of this paper is on the following set of the ordinary differential equations with a periodic forcing:

$$(2.1) \quad \begin{cases} \dot{x} = x(1 - r^2) - \alpha xz + \beta xz^2 + \gamma(1 - x) \sin(2\omega t) \\ \dot{y} = y(1 - r^2) + \alpha yz + \beta yz^2 \\ \dot{z} = z(1 - r^2) - \alpha(y^2 - x^2) - \beta z(x^2 + y^2) \end{cases}$$

where

$$r^2 = x^2 + y^2 + z^2, \quad \beta < 0 < \alpha, \quad \beta^2 < 8\alpha^2 \quad \Rightarrow \quad |\beta| < \alpha.$$

The amplitude of the perturbing term is governed by  $\gamma > 0$ . We have chosen the perturbing term

$$\gamma(1 - x) \sin(2\omega t).$$

It appears only in the first coordinate for two reasons: first, it simplifies the computations. Secondly, it allows comparison with previous work by other authors [3, 6, 12, 24, 31]. We denote the vector field associated to (2.1) by  $F_\gamma$ .

**Remark 1.** *The perturbation term  $\sin(2\omega t)$  may be replaced by  $f(2\omega t)$  where  $f$  is any  $2\pi$ -periodic and continuously differentiable function. In some places we use the property  $f''(t) = -4\omega^2 f(t)$ .*

**2.1. The unperturbed system ( $\gamma = 0$ ).** The dynamics associated to this equation has been systematically studied in [6]. For the sake of completeness, we recall its main properties. The vector field  $F_0$  has two symmetries of order 2:

$$\kappa_1(x, y, z) = (-x, y, z) \quad \text{and} \quad \kappa_2(x, y, z) = (x, -y, z)$$

forming a symmetry group isomorphic to  $\mathbf{Z}_2 \oplus \mathbf{Z}_2$ . The symmetry  $\kappa_2$  remains after the perturbation governed by  $\gamma$ . The unit sphere  $\mathbf{S}^2$  is flow-invariant and globally attracting. The points  $\mathbf{v} = (0, 0, 1)$  and  $\mathbf{w} = (0, 0, -1)$  are equilibria. From the symmetries  $\mathbf{Z}_2 \oplus \mathbf{Z}_2$ , it follows that the planes  $x = 0$  and  $y = 0$  are flow-invariant, and hence they meet  $\mathbf{S}^2$  in two flow-invariant circles connecting the equilibria  $(0, 0, \pm 1)$  – see Figure 1. Since  $\beta < 0 < \alpha$  and  $\beta^2 < 8\alpha^2$ , then these two equilibria are saddles, and there are heteroclinic trajectories going from each equilibrium to the other one. More precisely, the expanding and contracting eigenvalues  $E_p$  and  $C_p$  of the derivative of the vector field  $F_0$  at  $p \in \{\mathbf{v}, \mathbf{w}\}$  are:

$$E_{\mathbf{v}} = E_{\mathbf{w}} = \alpha + \beta > 0 \quad \text{and} \quad C_{\mathbf{v}} = C_{\mathbf{w}} = \beta - \alpha < 0,$$

with  $\hat{\delta} = \frac{C_{\mathbf{v}}}{E_{\mathbf{v}}} = \frac{C_{\mathbf{w}}}{E_{\mathbf{w}}} = \frac{|\beta - \alpha|}{\alpha + \beta} = \frac{\alpha - \beta}{\alpha + \beta}$ . The origin is a repellor.

Considering the system restricted to  $\mathbf{S}^2$ , equivariance forces the invariant manifolds in  $\mathbf{S}^2$  of  $\mathbf{v}$  and  $\mathbf{w}$  to be in a very special position: they coincide. In  $\mathbf{S}^2$ , the invariant manifolds of  $\mathbf{v}$  and  $\mathbf{w}$  are one-dimensional and contained in the invariant circles  $Fix(\mathbf{Z}_2(\kappa_j)) \cap \mathbf{S}^2$ ,  $j = 1, 2$ , giving rise to a heteroclinic network  $\Sigma_0$ . In the restriction to each of the invariant planes  $Fix(\kappa_j)$ ,  $j = 1, 2$  the equilibria  $\mathbf{v}$ ,  $\mathbf{w}$  have a saddle-sink connection, so this network is persistent under perturbations that preserve the symmetry, and in this sense it is robust.

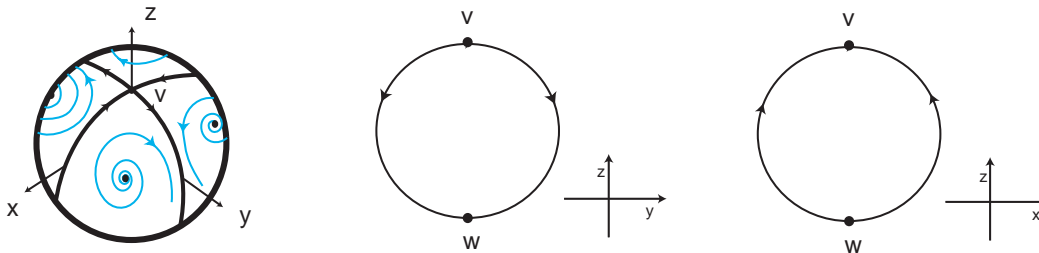


FIGURE 1. Sketch of the heteroclinic connections when  $\gamma = 0$  and  $\alpha > 0$ . When  $\alpha < 0$ , the arrows reverse orientation.

For all non-equilibrium points  $p \in \text{Fix}(\kappa_1) \cap \mathbf{S}^2$ , we have  $\omega(p) = \{\mathbf{w}\}$ , whereas for  $p \in \text{Fix}(\kappa_2) \cap \mathbf{S}^2$ , we have  $\omega(p) = \{\mathbf{v}\}$ , as in Figure 1.

The heteroclinic network  $\Sigma_0$  is asymptotically stable by the Krupa and Melbourne criterion [16, 17]. Note that:

$$\delta = (\hat{\delta})^2 = \frac{C_{\mathbf{v}} C_{\mathbf{w}}}{E_{\mathbf{v}} E_{\mathbf{w}}} = \frac{(\beta - \alpha)^2}{(\alpha + \beta)^2} > 1.$$

The constant  $\delta$  measures the strength of attraction of the cycle in the absence of perturbations. There are no periodic solutions near  $\Sigma_0$  because  $\delta > 1$ . Typical trajectories near the heteroclinic network  $\Sigma_0$  spend increasing amounts of time near each saddle point on each occasion they return close to it. In some places we assume that we are in the weakly attracting case  $\delta \gtrsim 1$ , we make the assumption explicitly when it is used. The case  $\delta = 1$ ,  $\gamma = 0$  corresponds to a *resonant bifurcation* of the robust heteroclinic cycle – this case has been explored by Postlethwaite and Dawes in [21, 22].

**2.2. A pull-back attractor for small  $\gamma$ .** Kloeden and Rasmussen [14] have results connecting attractors for autonomous systems and their perturbations, that may be applied here. We have that  $\Sigma_0$  is a global attractor of the autonomous flow ( $\gamma = 0$ ), the vector field  $F_0$  is uniformly Lipschitz and the periodic perturbation term  $\sin(2\omega t)$  is limited. Then Section 11 of [14] allows us to conclude that the non-autonomous system (2.1) generates a *process* which has a pullback attractor  $\Sigma_\gamma$  such that

$$\forall t \in \mathbf{R}, \quad \lim_{\gamma \rightarrow 0} \text{dist}(\Sigma_t^\gamma, \Sigma_0) = 0,$$

where  $\text{dist}$  is the euclidean distance on  $\mathbf{R}^3$ . Moreover, for a given  $\gamma > 0$ , the sets  $\Sigma_t^\gamma$  have the same Hausdorff dimension for all  $t \in \mathbf{R}$ . This suggests that solutions of the perturbed system (2.1) should make excursions around the ghost of  $\Sigma_0$ . In this article we explore the resulting dynamics.

Dawes and T.-L. Tsai [12, 30, 31], presented preliminary results on the perturbation of the example studied in [13]. They identified distinct dynamical regimes depending on whether  $\delta > 1$  is or not close to 1. Here we deal with the case  $\delta > 1$  in general. Our results provide insight into the dynamics of a non-autonomous periodic forcing of an autonomous equation with a compact attractor.

Our purpose in writing this paper is not only to point out the range of phenomena that can occur when simple non-linear equations are periodically forced, but to bring to the foreground the techniques that have allowed us to reach these conclusions in a relatively straightforward manner. These techniques are clearly not limited to the systems considered here. It is our hope that they will find applications in other dynamical systems, particularly those that arise naturally from mechanics or physics.

**2.3. Main results and structure of the paper.** We now describe briefly the main results and the contents of this paper. We provide informal statements of the results, that will be made rigorous in the course of the exposition. Since there is a large number of constants and parameters used in the article, we have included a list of notation as an appendix.

Expressions for the first return map to a section transverse to the connection  $[\mathbf{w} \rightarrow \mathbf{v}]$  are obtained in Section 3 for the case  $\gamma = 0$  and in Section 4 for the general case.

We linearise the autonomous equations around the equilibria in § 3.1 to construct a first return map. In Section 4, we begin by presenting a systematic calculation of the first return map for the robust heteroclinic cycle subjected to the non-negative periodic forcing function  $f(2\omega t) = \sin(2\omega t)$ . By including the time-dependent terms through all steps in the calculation, we obtain a first return map, that can be quantitatively compared to the dynamics of the original differential equations associated to  $F_0$  – see Remarks 3, 4 and 6. These comparisons show that the new return map associated to  $F_\gamma$  captures the dynamics well. The Poincaré map for (2.1), described in Theorem A, yields a description of the dynamics in terms of a two-dimensional map for the  $y$ -coordinate and the return time  $s$  at which trajectories reach the cross-section:

**Theorem A.** *In the weakly attracting case  $\delta \gtrsim 1$ , the first return map  $G$  to a given cross-section, of the flow defined by (2.1), may be approximated by a map of the form:*

$$G(s, y) = \left( s - \frac{\ln y}{K}, y^\delta + \gamma(1 + k_1 \sin(2\omega s)) \right) = (g_1(s, y), g_2(s, y)).$$

The values of the constants for Theorem A are given in the Appendix. Theorem A is proved in Section 4. Although this result is valid for the weakly attracting case, we may study the dynamics of  $G$  for all  $\delta > 1$ . The expression of  $G$  coincides with that obtained by Tsai and Dawes [31] for a different system, here we clarify and extend their results. Note that, because  $g_2$  is periodic in the variable  $s$ , the natural phase space for  $G$  is the cylinder

$$(2.2) \quad \mathcal{C} = \{(s, y) : y > 0, \quad s \in \mathbf{R} \pmod{\pi/\omega}\}.$$

The consequences of the interaction between  $\gamma$  and  $k_1$  in the original system are not trivial. In the weakly attracting case, if  $\gamma > 0$  is small and  $k_1 = 0$ , then the map  $G$  has both stable and unstable fixed points (corresponding to stable/unstable periodic solutions for the flow), say  $\hat{y}$  and  $\tilde{y}$ . For the non-autonomous equation (2.1), solutions might fluctuate by small amounts near the periodic orbit of an amplitude that would be anticipated from considering the time-averaged value of the forcing function. Based on the Annulus Principle [4], we obtain:

**Theorem B.** *There is an open set of parameters for which the maximal attractor for  $G$  is an invariant closed curve not contractible on the cylinder.*

The precise statement of Theorem B and its proof are treated in Section 5.

Section 6 is concerned with bifurcation and stability of periodic solutions of (2.1). For this, we first introduce an auxiliary parameter  $T$  and look for fixed points of  $\mathcal{G}_T(s, y) = G(s, y) - (T, 0)$ . A first step is the following:

**Proposition C.** *Consider the problem of finding fixed points of  $\mathcal{G}_T(s, y)$  with  $T \geq 0$ ,  $k_1 > 0$ ,  $\gamma > 0$ . The curves  $k_1 = 1$  and  $\gamma(1 - k_1) = M$  and  $\gamma(1 + k_1) = M$  with  $M = \delta^{\frac{1}{1-\delta}} - \delta^{\frac{\delta}{1-\delta}}$  separate the first quadrant of the  $(k_1, \gamma)$ -plane into five regions (see Figure 2) corresponding to the following behaviour:*

- (1)  $k_1 \in (0, 1)$  and  $M < \gamma(1 - k_1)$  — there are no fixed points;
- (2)  $k_1 \in (0, 1)$  and  $\gamma(1 - k_1) < M < \gamma(1 + k_1)$  — there are fixed points for each  $T$  in a closed interval;
- (3)  $k_1 \in (0, 1)$  and  $\gamma(1 + k_1) < M$  — there are fixed points for each  $T$  in the union of two disjoint closed intervals;
- (4)  $k_1 > 1$  and  $M < \gamma(1 + k_1)$  — there are fixed points for each  $T \in \mathbf{R}^+$ ;
- (5)  $k_1 > 1$  and  $\gamma(1 + k_1) < M$  — there are fixed points for each  $T$  in the complement of a limited open interval.

Moreover, when fixed points exist for  $T$  in an interval, then there are two fixed points for each  $T$  in the interior of the interval and only one for  $T$  in the boundary.

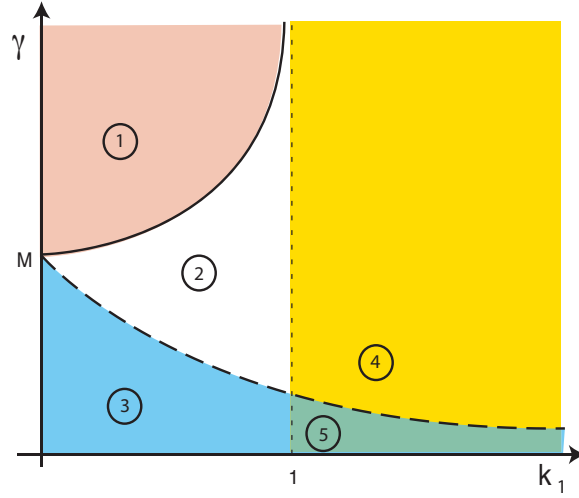


FIGURE 2. Bifurcation diagram on  $(k_1, \gamma)$ -plane for the fixed points of  $\mathcal{G}_T(s, y)$ : the solid line is  $\gamma = M/(1 - k_1)$ , the dashed line is  $\gamma = M/(1 + k_1)$ . Numbering corresponds to the cases in Proposition C.

Besides the finding of fixed points of  $\mathcal{G}_T(s, y)$ , in Section 6 we also discuss their stability and bifurcations between the different regions of the parameter space  $(T, k_1, \gamma)$ .

**Corollary D.** For  $k_1 > 0$ ,  $\gamma > 0$ ,  $\gamma = M/(1 \pm k_1)$ , fixed points of  $\mathcal{G}_T(s, y)$  undergo saddle-node bifurcations on the surfaces in the three dimensional parameter space  $(T, k_1, \gamma)$  given by

$$e^{-KT_j} - e^{-\delta KT_j} = \gamma(1 + k_1) \quad \forall k_1 \quad \text{and if } k_1 > 1 \text{ then also } e^{-KT_j} - e^{-\delta KT_j} = \gamma(1 - k_1).$$

In this context, we find in § 6.3 an organising centre for the dynamics of  $\mathcal{G}_T$  as follows:

**Theorem E.** There are curves in the three dimensional parameter space  $(T, k_1, \gamma)$  where fixed points of  $\mathcal{G}_T(s, y)$  undergo a discrete-time Bogdanov-Takens bifurcation, a single curve for  $k_1 > 1$ , two curves for  $0 < k_1 < 1$ .

In particular, we conclude that there are contractible closed  $\mathcal{G}_T$ -invariant curves arising at Hopf bifurcations and there exist small regions in parameter space where  $G$  has chaotic and non-hyperbolic dynamics. This is a consequence of the discrete-time Bogdanov-Takens bifurcation studied by Broer *et al* [7] and Yagasaki [33, § 3]. The stability of bifurcating solutions is studied in § 6.4.

In § 6.5 these results are used to find periodic solutions of the original differential equations whose period is an integer multiple of the period of the forcing terms — *frequency locked* solutions. This agrees well with numerics presented in [30]. We show their existence for different values of  $\omega$ , as well as the existence of invariant tori and chaotic regions. We also show that there is no gain in looking for different multiples  $n\pi/\omega$ ,  $n \in \mathbf{N}$  of the period, because we obtain essentially the same solution for all  $n$ . This is summarised as follows:

**Theorem F.** If  $\gamma(1 - k_1) < M$ , then there are two frequency locked solutions of (2.1) with period  $n\pi/\omega$ ,  $n \in \mathbf{N}$ , for the following values of  $\omega$ , according to the regions in Proposition C:

- (2)  $\omega \in (n\pi/T_2, n\pi/T_1)$ ;
- (3)  $\omega \in (n\pi/T_2, n\pi/T_1)$  and  $\omega \in (n\pi/T_4, n\pi/T_3)$ ;
- (5)  $\omega < n\pi/T_2$  and  $\omega > n\pi/T_1$ ;
- (4) all  $\omega > 0$ ;

where the  $T_j$  for  $j = 1, \dots, 4$  have the values of Proposition C.

There are values of  $(k_1, \gamma)$  and values  $\omega_{H_1} < \omega_{H_2}$  and  $\omega_{h_1} < \omega_{h_2}$  such that, for each  $n \in \mathbf{N}$ :

- for  $\omega \in (n\omega_{H_1}, n\omega_{H_2})$  there is a  $G$ -invariant curve on the cylinder that corresponds to a frequency locked invariant torus for (2.1);
- for  $\omega \in (n\omega_{h_1}, n\omega_{h_2})$  there is a  $G$ -invariant set with dynamics conjugate to a shift on a finite number of symbols, and hence there is a frequency locked suspended horseshoe for (2.1).

Moreover,  $(s_1, y)$  is a fixed point of  $G$  in the cylinder, corresponding to a periodic solution of (2.1) with period  $\pi/\omega$  if and only if  $(\frac{s_1}{n}, y)$  is a fixed point of  $G$  in the cylinder, corresponding to a periodic solution of (2.1) with period  $\pi/n\omega$  for arbitrary  $n \in \mathbf{N}$ .

Finally we analyse in Section 7 the dynamics near special solutions with frequency locked periods, called the *centres of frequency locking*.

**Theorem G.** *Near the centre of the frequency locking, the dynamics of  $G(s, y)$  is approximated by the discretisation of the equation for a damped pendulum with constant torque*

$$\theta'' + B\theta' + \sin \theta = A \quad \text{with} \quad A, B > 0.$$

An explicit expression for  $A$  and  $B$  in terms of the parameters in  $G$  is given in Section 7. The effects of time-periodic forcing on the damped pendulum was extensively studied by Andronov *et al* [1] and we use their results to obtain information about our problem.

As a corollary we conclude that there is an open region in the space of parameters where solutions of (2.1) are attracted either to a stable non-trivial periodic solution or to an attracting torus. These two flow-invariant sets may coexist and attract open sets of trajectories. We say that the system exhibits *bistability*. The physical meaning is explained in [11].

Dynamics similar to that which we have described is expected to occur generically near periodically forced robust weakly attracting heteroclinic cycles. This is why the result of our computations may be applied to other similar cases. The understanding of the effects of different classes of perturbation is far from being done. We finish the article with a short discussion in Section 8 of the consequences of our findings, both for the map  $G(s, y)$  and for the equation (2.1).

### 3. TIME-INDEPENDENT FIRST RETURN MAP

We will define four cross-sections transverse to all trajectories in a neighbourhood of  $\Sigma_0$ . Repeated intersections to a fixed cross-section define a return map from the section to itself; studying the dynamics of this map enables us to understand the dynamics of trajectories near  $\Sigma_0$ .

We construct the return map as the composition of two types of map: *local maps* within neighbourhoods of the saddle-type equilibrium points where the dynamics can be well approximated by the flow of the linearised equations, and transition maps from one neighbourhood to another (also called *global maps*).

Near the equilibrium  $\mathbf{v}$ , the cross-sections are denoted  $In(\mathbf{v})$  and  $Out(\mathbf{v})$ .

**3.1. Linearisation.** By Samovol's Theorem [27], around the saddles  $\mathbf{v}$  and  $\mathbf{w}$ , the vector field  $F_0$  is  $C^1$ -conjugate to its linear part, since there are no resonances of order 1. In local coordinates  $(x, y, w)$  the linearisation of (2.1) with  $\gamma = 0$ , at  $\mathbf{v}$  and  $\mathbf{w}$  takes the form

$$(3.3) \quad \begin{cases} \dot{x} = (\beta - \alpha)x \\ \dot{y} = (\alpha + \beta)y \\ \dot{w} = -2(1 + w) \end{cases}$$

where  $z = 1 + w$  near  $\mathbf{v}$  and  $z = w - 1$  near  $\mathbf{w}$  with  $|w|$  small.

**3.2. The cross-sections.** Consider cubic neighbourhoods  $V$  and  $W$  in  $\mathbf{R}^3$  of  $\mathbf{v}$  and  $\mathbf{w}$ , respectively, given in the coordinates of (3.3) by (see Figure 3):

$$\{(x, y, w), |x| < \varepsilon, |y| < \varepsilon, |w| < \varepsilon\}$$

for  $\varepsilon > 0$  small. The boundary of  $V$  consists of six connected components.

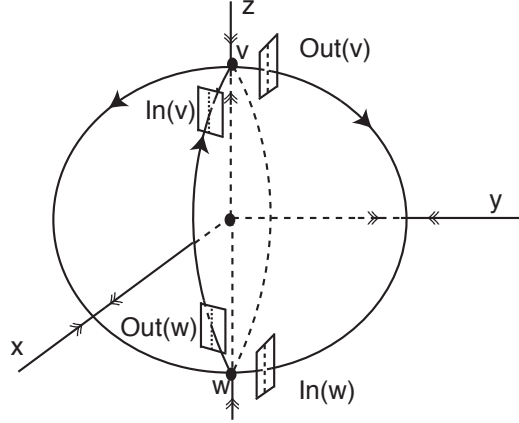


FIGURE 3. Trajectories not on  $W^s(\mathbf{v})$  reach the cross-section  $In(\mathbf{v})$ , go transversely through it, then pass near  $\mathbf{v}$  and again go transversely through the cross-section  $Out(\mathbf{v})$ . After this they continue to a neighbourhood of  $\mathbf{w}$ , moving transversely through the cross-sections  $In(\mathbf{w})$  and  $Out(\mathbf{w})$  and finally returning to  $In(\mathbf{v})$ .

- Two squares, the top and the bottom of the cube parametrised by  $w = \pm\varepsilon$ , where the flow enters  $V$  in the radial direction.
- The set of points that go inside  $V$  in positive time, that has two components, one of which is

$$In(\mathbf{v}) = \{(\varepsilon, y, z), |y| < \varepsilon, z = 1 + w, |w| < \varepsilon\} \mapsto (y_1, w_1).$$

- The set of points that go outside  $V$  in positive time, with two components, one of which is

$$Out(\mathbf{v}) = \{(x, \varepsilon, z), |x| < \varepsilon, z = 1 + w, |w| < \varepsilon\} \mapsto (\hat{x}_1, \hat{w}_1).$$

Similarly, the boundary of  $W$  consists of six connected components.

- Two squares, the top and the bottom of the cube parametrised by  $w = \pm\varepsilon$ , where the flow enters  $W$  in the radial direction.
- The set of points that go inside  $W$  in positive time, that has two components, one of which is

$$In(\mathbf{w}) = \{(x, \varepsilon, z), |x| < \varepsilon, z = -1 + w, |w| < \varepsilon\} \mapsto (x_2, w_2).$$

- The set of points that go outside  $W$  in positive time, with two components, one of which is

$$Out(\mathbf{w}) = \{(\varepsilon, y, z), |y| < \varepsilon, z = 1 + w, |w| < \varepsilon\} \mapsto (\hat{y}_2, \hat{w}_2).$$

**3.3. Local map near  $\mathbf{v}$ .** The solution of the linearised system (3.3) near  $\mathbf{v}$  with initial conditions  $y_1, z_1$  in  $In(\mathbf{v})$  is:

$$\begin{cases} x(t) = \varepsilon e^{(\beta-\alpha)t} \\ y(t) = y_1 e^{(\alpha+\beta)t} \\ z(t) = z_1 e^{-2t} \end{cases}$$

The time of flight  $T_1$  of a trajectory inside  $V$  is the solution of

$$(3.4) \quad y(T_1) = \varepsilon \Leftrightarrow y_1 e^{(\alpha+\beta)T_1} = \varepsilon \Leftrightarrow T_1 = s + \frac{1}{\alpha + \beta} \ln \left( \frac{\varepsilon}{y_1} \right).$$

Therefore, the transition map  $\Phi_{\mathbf{v}} : In(\mathbf{v}) \rightarrow Out(\mathbf{v})$  in coordinates  $(y_1, z_1) \in In(\mathbf{v})$  and  $(\hat{x}_1, \hat{z}_1) \in Out(\mathbf{v})$  is:

$$(3.5) \quad \Phi_{\mathbf{v}}(y_1, z_1) = \left( \varepsilon^{1 + \frac{\beta-\alpha}{\alpha+\beta}} y_1^{\frac{\alpha-\beta}{\alpha+\beta}}, z_1 \varepsilon^{-\frac{2}{\alpha+\beta}} y_1^{\frac{2}{\alpha+\beta}} \right) = (\hat{x}_1, \hat{z}_1)$$

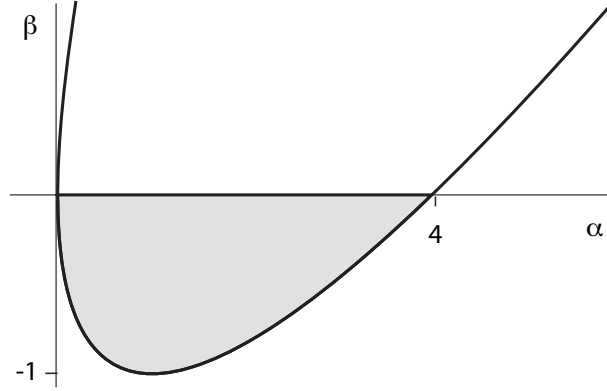


FIGURE 4. In the grey region,  $(\alpha - \beta)^2 - 4\alpha < 0$  for  $\alpha > 0$ ,  $\beta < 0$ , hence in  $G_0(y, z_1)$  the exponent of  $y$  in the first coordinate is smaller than in the second coordinate. The inequality is reversed below the parabola.

**3.4. Local map near  $\mathbf{w}$ .** The solution of the linearised system (3.3) near  $\mathbf{w}$  with initial conditions  $x_2, z_2$  in  $In(\mathbf{w})$  is:

$$\begin{cases} x(t) = x_2 e^{(\alpha+\beta)t} \\ y(t) = \varepsilon e^{(\beta-\alpha)t} \\ z(t) = z_2 e^{-2t} \end{cases}$$

The time of flight  $T_2$  from  $In(\mathbf{w})$  to  $Out(\mathbf{w})$  is the solution of  $x(T_2) = \varepsilon$ :

$$x_2 e^{(\alpha+\beta)(T_2-s)} = \varepsilon \quad \Leftrightarrow \quad T_2 = s + \frac{1}{\alpha + \beta} \ln \left( \frac{\varepsilon}{x_2} \right)$$

in coordinates  $(x_2, z_2) \in In(\mathbf{w})$  and  $(\hat{y}_2, \hat{z}_2) \in Out(\mathbf{w})$  is:

$$(3.6) \quad \Phi_{\mathbf{w}}(x_2, z_2) = \left( \varepsilon^{1+\frac{\beta-\alpha}{\alpha+\beta}} x_2^{\frac{\alpha-\beta}{\alpha+\beta}}, z_2 \varepsilon^{-\frac{2}{\alpha+\beta}} x_2^{\frac{2}{\alpha+\beta}} \right) = (\hat{y}_2, \hat{z}_2)$$

**3.5. The global maps.** An approximation to the maps

$$\Psi_{\mathbf{vw}} : Out(\mathbf{v}) \rightarrow In(\mathbf{w}) \quad \text{and} \quad \Psi_{\mathbf{wv}} : Out(\mathbf{w}) \rightarrow In(\mathbf{v})$$

is to take them as the identity. In coordinates we obtain

$$\Psi_{\mathbf{vw}}(\hat{x}_1, \hat{z}_1) \mapsto (x_2, z_2) = (\hat{x}_1, \hat{z}_1) \quad \text{and} \quad \Psi_{\mathbf{wv}}(\hat{y}_2, \hat{z}_2) \mapsto (y_1, z_1) = (\hat{y}_2, \hat{z}_2)$$

**3.6. First return map for the unperturbed equation.** The first return map  $G_0$  to  $In(\mathbf{v})$  is well defined at all points  $(y_1, w_1) \in In(\mathbf{v}) \setminus W_{loc}^s(\mathbf{v})$ . After a linear rescaling of the variables, we may assume that  $\varepsilon = 1$  and obtain

$$(3.7) \quad G_0(y_1, z_1) = \left( y_1^\delta, z_1 y_1^{\frac{4\alpha}{(\alpha+\beta)^2}} \right).$$

Either the first or the second coordinate dominates, depending on the relative size of the exponents in  $y_1$ , *i.e.* depending on the sign of  $(\alpha - \beta)^2 - 4\alpha$ , see Figure 4. The transition between the boundaries of  $V$  and  $W$  occurs in a flow-box, hence the transition time is limited above and below. We assume the transitions far from the equilibria are instantaneous, and then the time of the first return of the point  $(y_1, z_1)$  with  $y_1 \neq 0$  is given by  $T_1 + T_2 = -\frac{2\alpha}{(\alpha + \beta)^2} \ln y_1$ . Taking into account the transition times out of  $V$  and  $W$  would approximately change the value of  $T_1 + T_2$  by a constant.

## 4. TIME-DEPENDENT FIRST RETURN

The aim of this section is to obtain an expression for the first return map to  $In(\mathbf{v})$  when  $\gamma \neq 0$ , that will be denoted by  $G$ . When  $\gamma = 0$ , the map  $G$  should coincide with  $G_0$  defined in (3.7). Specifically, we prove

**Theorem 1.** *If  $\gamma \geq 0$ ,  $\delta \gtrsim 1$  and  $(\alpha - \beta)^2 < 4\alpha$ , the first return map  $G$  to the cross-section  $In(\mathbf{v})$ , of the flow defined by (2.1), may be approximated by the map:*

$$(4.8) \quad G(s, y) = \left( s - K \ln y, y^\delta + \gamma(1 + k_1 \sin(2\omega s)) \right) = (g_1(s, y), g_2(s, y))$$

where  $K = \frac{2\alpha}{(\alpha + \beta)^2}$  and  $k_1 > 0$ .

Because of the time-periodic perturbation, the local linearisation now includes time-dependent terms that are important in the accurate calculation of the local map.

At each step, we calculate not only the point where a solution hits each cross-section but also the time the solution takes to move between cross-sections. As in § 3.6, the time spent close to the connections is small compared with the time spent near the equilibria, especially when  $\gamma > 0$  is small. This time is not taken into account in the calculations. Note that the equilibria for the vector field  $F_0$  (associated to the equation (2.1) when  $\gamma = 0$ ) are no longer equilibria for  $F_\gamma$ , but the cross-sections remain transverse.

**4.1. Linearization.** The linearisation near  $\mathbf{v}$  and  $\mathbf{w}$  may be written as:

$$(4.9) \quad \begin{cases} \dot{x} = (\beta - \alpha)x - \gamma f(2\omega t) \\ \dot{y} = (\alpha + \beta)y \\ \dot{z} = -2z \end{cases}$$

and

$$(4.10) \quad \begin{cases} \dot{x} = (\alpha + \beta)x - \gamma f(2\omega t) \\ \dot{y} = (\beta - \alpha)y \\ \dot{z} = -2z \end{cases}$$

respectively, with  $f(2\omega t) = \sin(2\omega t)$ .

Equation (2.1) may be written in the form  $\dot{X} = \mathcal{A}X + R(X) - \gamma f(2\omega t)$  for  $X = (x, y, z)$  and where  $\dot{X} = \mathcal{A}X - \gamma f(2\omega t)$  is any of the equations (4.9) or (4.10). In this form we have that the constant matrix  $\mathcal{A}$  has no eigenvalues with a zero real part, the perturbation  $\gamma f(2\omega t)$  is limited and the non-linear part  $R(X)$  is limited and uniformly Lipschitz in a compact neighbourhood of  $\mathbf{S}^2$ . Under these conditions, we may use Palmer's Theorem [20, pp 754] to conclude that there is a small neighbourhood of  $\mathbf{v}$  and  $\mathbf{w}$  where the vector field is  $C^1$  conjugate to its linear part. As before, let us label the neighbourhoods by  $V$  and  $W$ , respectively. The terminology for the boundary sections in  $V$  and  $W$  will be the same as in § 3.2.

**Remark 2.** *If  $k, \gamma \in \mathbf{R}$ , according to the Lagrange method of variation of parameters – see [29, pp 842], the general solution of:*

$$\begin{cases} \dot{x} = kx + \gamma g(t) \\ x(s) = x_1 \end{cases}$$

is

$$x(t, s) = x_1 e^{k(t-s)} \Psi(t, s) \quad \text{where} \quad \Psi(t) = 1 + \frac{\gamma}{x_1} \int_s^t e^{-k(\tau-s)} g(\tau) d\tau.$$

**4.2. Local map near  $\mathbf{v}$ .** Let us describe the general solution of (4.9). For  $z = 1 + w$  we get  $\dot{w} = -2(1 + w)$ . By Remark 2, the solution of the linearised system (4.9) near  $\mathbf{v}$  is:

$$(4.11) \quad \begin{cases} x(t, s) = \varepsilon e^{(\beta-\alpha)(t-s)} \left( 1 - \frac{\gamma}{\varepsilon} \int_s^t e^{-(\beta-\alpha)(\tau-s)} f(2\omega\tau) d\tau \right) \\ y(t, s) = y_1 e^{(\alpha+\beta)(t-s)} \\ w(t, s) = (w_1 + 1) e^{-2(t-s)} - 1 \end{cases}$$

where  $y_1, w_1$  are the initial conditions in  $In(\mathbf{v})$ . The time of flight is the solution of  $y(T_1) = \varepsilon$ :

$$y(T_1) = \varepsilon \Leftrightarrow y_1 e^{(\alpha+\beta)(T_1-s)} = \varepsilon \Leftrightarrow \ln \left( \frac{\varepsilon}{y_1} \right) = (\alpha + \beta)(T_1 - s).$$

Therefore, the arrival time depends on  $s$  and it is given by:

$$(4.12) \quad T_1 = s + \ln \left( \frac{\varepsilon}{y_1} \right)^{\frac{1}{\alpha+\beta}} = s + \frac{1}{\alpha + \beta} \ln \left( \frac{\varepsilon}{y_1} \right).$$

In particular, we may write:

$$w(T_1, s) = (w_1 + 1) e^{-2(T_1-s)} - 1$$

which is equivalent to

$$w(T_1, s) = (w_1 + 1) \left( \frac{\varepsilon}{y_1} \right)^{\frac{-2}{\alpha+\beta}} - 1.$$

Replacing  $t$  by  $T_1$  of (4.12) in the first equation of (4.11), we get:

$$x(T_1, s) = \varepsilon \left( \frac{\varepsilon}{y_1} \right)^{-\widehat{\delta}} \left( 1 - \frac{\gamma}{\varepsilon} \int_s^{T_1} e^{-(\beta-\alpha)(\tau-s)} f(2\omega\tau) d\tau \right)$$

where  $\widehat{\delta} = \frac{C_{\mathbf{v}}}{E_{\mathbf{v}}} = \frac{|\beta-\alpha|}{\alpha+\beta} = \frac{\alpha-\beta}{\alpha+\beta}$  as defined in § 2.1. Therefore, we may write:

$$\Phi_{\mathbf{v}}(s, y_1, w_1) = \begin{pmatrix} s + \frac{1}{\alpha+\beta} \ln \left( \frac{\varepsilon}{y_1} \right) \\ \varepsilon^{-\widehat{\delta}+1} y_1^{\widehat{\delta}} \left( 1 - \frac{\gamma}{\varepsilon} \int_s^{T_1} e^{-(\beta-\alpha)(\tau-s)} f(2\omega\tau) d\tau \right) \\ (w_1 + 1) \left( \frac{\varepsilon}{y_1} \right)^{\frac{-2}{\alpha+\beta}} - 1 \end{pmatrix} = (T_1, \widehat{x}_1, \widehat{w}_1).$$

**Remark 3.** Note that when  $\varepsilon = 1$  and  $\gamma = 0$ , the first, second and third components coincide with formulas (3.4) and the second component of (3.5).

**4.3. Local map near  $\mathbf{w}$ .** The treatment of (4.10) is similar to § 4.2. From  $z = -1 + w$ , it follows that  $\dot{w} = -2(w - 1)$ . The solution of (4.10) is:

$$\begin{cases} x(t) = x_2 e^{(\alpha+\beta)(t-s)} \left( 1 - \frac{\gamma}{x_2} \int_s^t e^{-(\alpha+\beta)(\tau-s)} f(2\omega\tau) d\tau \right) \\ y(t) = \varepsilon e^{(\beta-\alpha)(t-s)} \\ w(t) = (w_2 - 1) e^{-2(t-s)} + 1. \end{cases}$$

The time of flight  $T_2$  from  $In(\mathbf{w})$  to  $Out(\mathbf{w})$  is the solution of  $x_2(T_2) = \varepsilon$ :

$$(4.13) \quad x_2 e^{(\alpha+\beta)(T_2-s)} \left( 1 - \frac{\gamma}{x_2} \int_s^{T_2} e^{-(\alpha+\beta)(\tau-s)} f(2\omega\tau) d\tau \right) = \varepsilon.$$

This is difficult to solve, so we compute the Taylor expansion of  $T_2$  as function of  $\gamma$ . It is easy to see that  $T_2(0) = s + \ln \left( \frac{\varepsilon}{x_2} \right)^{\frac{1}{\alpha+\beta}}$ . Differentiating equation (4.13) with respect to  $\gamma$ , and evaluating at  $\gamma = 0$ , it yields:

$$0 = T_2'(0) x_2 (\alpha + \beta) e^{(\alpha+\beta)(T_2(0)-s)} - e^{(\alpha+\beta)(T_2(0)-s)} \int_s^{T_2(0)} e^{-(\alpha+\beta)(\tau-s)} f(2\omega\tau) d\tau,$$

implying that:

$$T_2'(0) = \frac{1}{x_2(\alpha + \beta)} \int_s^{T_2(0)} e^{-(\alpha+\beta)(\tau-s)} f(2\omega\tau) d\tau.$$

Thus, truncating at second order in  $\gamma$  we obtain:

$$T_2(\gamma) \approx s + \frac{1}{\alpha + \beta} \ln\left(\frac{\varepsilon}{x_2}\right) + \gamma \left[ \frac{1}{x_2(\alpha + \beta)} \int_s^{T_2(0)} e^{-(\alpha+\beta)(\tau-s)} f(2\omega\tau) d\tau \right] + O(\gamma^2).$$

Since  $y(t) = \varepsilon e^{(\beta-\alpha)(t-s)}$ , setting  $\hat{\delta} = \frac{C_{\mathbf{w}}}{E_{\mathbf{w}}} = \frac{\alpha-\beta}{\alpha+\beta}$ , as in § 2.1, we get:

$$y(T_2(0)) = \varepsilon e^{(\beta-\alpha)\left(\frac{1}{\alpha+\beta} \ln\left(\frac{\varepsilon}{x_2}\right)\right)} = \varepsilon \left(\frac{x_2}{\varepsilon}\right)^{\hat{\delta}}$$

and then:

$$\begin{aligned} y_2'(0) &= \varepsilon(\beta - \alpha) e^{(\beta-\alpha)(T_2(0)-s)} T_2'(0) \\ &= \varepsilon(\beta - \alpha) \left(\frac{\varepsilon}{x_2}\right)^{-\hat{\delta}} \left[ \frac{1}{x_2(\alpha + \beta)} \int_s^{T_2(0)} e^{-(\alpha+\beta)(\tau-s)} f(2\omega\tau) d\tau \right] \\ &= \hat{\delta} \varepsilon^{1-\hat{\delta}} x_2^{\hat{\delta}-1} \int_s^{T_2(0)} e^{-(\alpha+\beta)(\tau-s)} f(2\omega\tau) d\tau. \end{aligned}$$

Adding up, we get:

$$y_2(\gamma) = (\varepsilon^{-\hat{\delta}+1} x_2^{\hat{\delta}}) + \gamma \left[ \hat{\delta} \varepsilon^{1-\hat{\delta}} x_2^{\hat{\delta}-1} \int_s^{T_2(0)} e^{-(\alpha+\beta)(\tau-s)} f(2\omega\tau) d\tau \right] + O(\gamma^2).$$

Concerning the coordinate  $w$ , we may write:

$$w(0) = (w_2 - 1) e^{-2(T_2(0)-s)} + 1 = (w_2 - 1) \left(\frac{\varepsilon}{x_2}\right)^{\frac{-2}{\alpha+\beta}} + 1.$$

On the other hand, the following equalities hold:

$$w'(0) = -2(w_2 - 1) e^{-2(T_2(0)-s)} T_2'(0) = -2(w_2 - 1) \left(\frac{\varepsilon}{x_2}\right)^{\frac{-2}{\alpha+\beta}} \left[ \frac{1}{x_2(\alpha + \beta)} \int_s^{T_2(0)} e^{-(\alpha+\beta)(\tau-s)} f(2\omega\tau) d\tau \right].$$

Therefore,  $\Phi_{\mathbf{w}}(s, x_2, w_2) = (T_2, \hat{y}_2, \hat{w}_2)$  is given by:

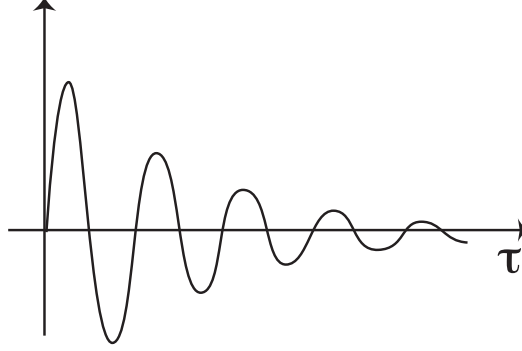
$$\left( \begin{array}{c} s + \frac{1}{\alpha+\beta} \ln\left(\frac{\varepsilon}{x_2}\right) + \gamma \left[ \frac{1}{x_2(\alpha+\beta)} \int_s^{T_2(0)} e^{-(\alpha+\beta)(\tau-s)} f(2\omega\tau) d\tau \right] \\ (\varepsilon^{-\hat{\delta}+1} x_2^{\hat{\delta}}) + \gamma \left[ \hat{\delta} \varepsilon^{1-\hat{\delta}} x_2^{\hat{\delta}-1} \int_s^{T_2(0)} e^{-(\alpha+\beta)(\tau-s)} f(2\omega\tau) d\tau \right] \\ 1 + (w_2 - 1) \left(\frac{\varepsilon}{x_2}\right)^{\frac{-2}{\alpha+\beta}} + \gamma \left[ -2(w_2 - 1) \left(\frac{\varepsilon}{x_2}\right)^{\frac{-2}{\alpha+\beta}} \left[ \frac{1}{x_2(\alpha+\beta)} \int_s^{T_2(0)} e^{-(\alpha+\beta)(\tau-s)} f(2\omega\tau) d\tau \right] \right] \end{array} \right) + O(\gamma^2).$$

**Remark 4.** When  $s = 0$ ,  $\varepsilon = 1$  and  $\gamma = 0$ , the last two components of the previous map coincide with the expression given in (3.6).

**4.4. Discussion of the time dependence.** We are assuming in (2.1) that  $\alpha + \beta > 0$ , hence the term  $e^{-(\alpha+\beta)\tau} f(2\omega\tau)$  that appears inside the integrals in  $\Phi_{\mathbf{w}}$  tends to zero as  $\tau$  goes to  $\infty$  – see Figure 5. For large times we may take the contribution of this integral to be time independent.

Setting

$$K_1 = \int_s^{T_2(0)} e^{-(\alpha+\beta)(\tau-s)} f(2\omega\tau) d\tau,$$

FIGURE 5. Graph of  $e^{-(\alpha+\beta)\tau} f(2\omega\tau)$  as a function of  $\tau$ .

we get

$$\Phi_{\mathbf{w}}(s, x_2, w_2) = \begin{pmatrix} s + \frac{1}{\alpha + \beta} \ln \left( \frac{\varepsilon}{x_2} \right) + \frac{\gamma K_1}{x_2(\alpha + \beta)} \\ \varepsilon^{1-\hat{\delta}} x_2^{\hat{\delta}} \left( 1 + \frac{\gamma K_1 \hat{\delta}}{x_2} \right) \\ 1 + (w_2 - 1) \left( \frac{\varepsilon}{x_2} \right)^{\frac{-2}{\alpha + \beta}} \left( 1 - \frac{2\gamma K_1}{x_2(\alpha + \beta)} \right) \end{pmatrix} = (T_2, \hat{y}_2, \hat{w}_2).$$

On the other hand, the assumptions in (2.1) also include  $\alpha > -\beta > 0$  implying that the coefficient  $-(\beta - \alpha) > 0$ . Hence the exponent  $-(\beta - \alpha)\tau$  that appears in  $\Phi_{\mathbf{v}}$  increases with  $\tau$  and the integral cannot be ignored. In order to obtain estimates for the integral, let  $I_A$ , for  $A > 0$ , be given by:

$$I_A = \int e^{-A(\tau-s)} f(2\omega\tau) d\tau.$$

**Lemma 2.** *If  $f''(t) = -f(t)$ , then:*

$$I_A = \frac{-A^2}{A^2 + 4\omega^2} e^{-A(\tau-s)} \left( \frac{1}{A} f(2\omega\tau) + \frac{2\omega}{A^2} f'(2\omega\tau) \right).$$

*Proof.* Integrating by parts twice, we obtain:

$$I_A = \frac{-1}{A} e^{-A(\tau-s)} f(2\omega\tau) - \frac{2\omega}{A^2} e^{-A(\tau-s)} f'(2\omega\tau) - \frac{4\omega^2}{A^2} I_A.$$

Hence,

$$\left( 1 + \frac{4\omega^2}{A^2} \right) I_A = -e^{-A(\tau-s)} \left( \frac{1}{A} f(2\omega\tau) + \frac{2\omega}{A^2} f'(2\omega\tau) \right)$$

which is equivalent to the expression in the statement.  $\square$

**Lemma 3.** *If  $f''(t) = -f(t)$  and  $T_1 = s + \frac{1}{\alpha + \beta} \ln \left( \frac{\varepsilon}{y_1} \right)$  as in the expression of  $\Phi_{\mathbf{v}}$ , we have*

$$\int_s^{T_1} e^{-(\beta-\alpha)(\tau-s)} f(2\omega\tau) d\tau = \frac{-(\beta-\alpha)^2}{(\beta-\alpha)^2 + 4\omega^2} \left[ \left( \frac{\varepsilon}{y_1} \right)^{\hat{\delta}} (c_1 f(2\omega T_1) + c_2 f'(2\omega T_1)) - (c_1 f(2\omega s) + c_2 f'(2\omega s)) \right]$$

where

$$c_1 = \frac{1}{\beta - \alpha} \quad \text{and} \quad c_2 = \frac{2\omega}{(\beta - \alpha)^2}.$$

*Proof.* First of all note that  $e^{-(\beta-\alpha)(T_1-s)} = \left(\frac{\varepsilon}{y_1}\right)^{\hat{\delta}}$ . Evaluating the expression of Lemma 2, with  $A = \beta - \alpha$ , in  $T_1$  and in  $s$  and tidying up, we obtain the result.  $\square$

**Remark 5.** *If  $f$  is an arbitrary periodic function, then Lemma 3 may be applied to each one of the terms of its Fourier expansion.*

**4.5. First return map.** From now on we return to the assumption  $f(2\omega s) = \sin 2\omega s$ . Hence  $f$  satisfies the hypothesis of Lemma 3 and the expression of  $\Phi_{\mathbf{v}}$  may be simplified. The second coordinate of  $\Phi_{\mathbf{v}}$  (see § 4.2 above) is

$$\hat{x}_1 = \varepsilon^{-\hat{\delta}+1} y_1^{\hat{\delta}} \left( 1 - \frac{\gamma}{\varepsilon} \int_s^{T_1} e^{-(\beta-\alpha)(\tau-s)} \sin(2\omega\tau) d\tau \right).$$

Using the expression in Lemma 3 yields  $\hat{x}_1 = \varepsilon^{-\hat{\delta}+1} y_1^{\hat{\delta}} + R$  where:

$$R = \frac{\gamma \varepsilon^{-\hat{\delta}+1} y_1^{\hat{\delta}} (\alpha - \beta)^2}{(\alpha - \beta)^2 + 4\omega^2} \left[ \left( \frac{\varepsilon}{y_1} \right)^{\hat{\delta}} (c_1 f(2\omega T_1) + c_2 f'(2\omega T_1)) - (c_1 f(2\omega s) + c_2 f'(2\omega s)) \right]$$

hence, for  $\varepsilon = 1$ ,

$$R = \frac{\gamma(\alpha - \beta)^2}{(\alpha - \beta)^2 + 4\omega^2} \left[ (c_1 f(2\omega T_1) + c_2 f'(2\omega T_1)) - y_1^{\hat{\delta}} \varepsilon^{-\hat{\delta}} (c_1 f(2\omega s) + c_2 f'(2\omega s)) \right].$$

For  $f(2\omega s) = \sin 2\omega s$ , the expression  $c_1 f(X) + c_2 f'(X)$  may be replaced by  $\hat{k} \sin(X - \hat{\theta})$ , for some  $\hat{\theta}$ . Using the expressions for  $c_1, c_2$  from Lemma 3 we get

$$\hat{k} = \sqrt{c_1^2 + c_2^2} = \frac{1}{(\alpha - \beta)^2} \sqrt{(\alpha - \beta)^2 + 4\omega^2}.$$

From now on, let us set:

$$\bar{k} = \frac{(\alpha - \beta)^2 \hat{k}}{(\alpha - \beta)^2 + 4\omega^2} = \frac{1}{\sqrt{(\alpha - \beta)^2 + 4\omega^2}}$$

hence

$$R = \bar{k} \gamma f(2\omega T_1 - \hat{\theta}) - y_1^{\hat{\delta}} \varepsilon^{-\hat{\delta}} \bar{k} \gamma f(2\omega s - \hat{\theta}).$$

Finally the whole expression for  $R$  may be rewritten as an approximation of  $\gamma \bar{k} \sin(2\omega T_1 - \theta)$  where the dependence of  $\bar{k}$  on  $y_1$  may be ignored for small  $y_1$  and  $\gamma$ . We shall ignore the phase shift term  $\theta$ , return to the usage  $f(t) = \sin t$  and rewriting the expressions in  $z$  instead of  $w$ , we use from now on the simplified expressions:

$$\Phi_{\mathbf{v}}(s, y_1, z_1) = \begin{pmatrix} s + \frac{1}{\alpha + \beta} \ln \left( \frac{\varepsilon}{y_1} \right) \\ \varepsilon^{-\hat{\delta}+1} y_1^{\hat{\delta}} + \gamma \bar{k} \sin(2\omega T_1) \\ z_1 \left( \frac{\varepsilon}{y_1} \right)^{\frac{-2}{\alpha + \beta}} \end{pmatrix} = (T_1, \hat{x}_1, \hat{z}_1)$$

and

$$\Phi_{\mathbf{w}}(s, x_2, z_2) = \begin{pmatrix} s + \frac{1}{\alpha + \beta} \ln \left( \frac{\varepsilon}{x_2} \right) + \frac{\gamma K_1}{x_2(\alpha + \beta)} \\ \varepsilon^{1-\hat{\delta}} x_2^{\hat{\delta}} \left( 1 + \frac{\gamma K_1 \hat{\delta}}{x_2} \right) \\ 1 + z_2 \left( \frac{\varepsilon}{x_2} \right)^{\frac{-2}{\alpha + \beta}} \left( 1 - \frac{2\gamma K_1}{x_2(\alpha + \beta)} \right) \end{pmatrix} = (T_2, \hat{y}_2, \hat{z}_2).$$

For the calculation of the first return map we take the transitions between the neighbourhoods  $V$  and  $W$  to be the identity, with  $\varepsilon = 1$ . The second coordinate  $\Phi_{\mathbf{w}}(\Phi_{\mathbf{v}})|_2$  of  $\Phi_{\mathbf{w}}(\Phi_{\mathbf{v}})$  is:

$$\Phi_{\mathbf{w}}(\Phi_{\mathbf{v}})|_2 = \left( y_1^{\widehat{\delta}} + \gamma \bar{k} \sin(2\omega T_1) \right)^{\widehat{\delta}} \left( 1 + \frac{\gamma K_1 \widehat{\delta}}{y_1^{\widehat{\delta}} + \gamma \bar{k} \sin(2\omega T_1)} \right).$$

Taking into account that  $\sum_{j=0}^{\infty} x^j = \frac{1}{1-x}$ , we expand the factor on the right to get:

$$1 + \frac{\gamma K_1 \widehat{\delta}}{y_1^{\widehat{\delta}} + \gamma \bar{k} \sin(2\omega T_1)} = 1 + \frac{\gamma K_1 \widehat{\delta}}{y_1^{\widehat{\delta}}} \left[ 1 - \frac{\gamma \bar{k} \sin(2\omega T_1)}{y_1^{\widehat{\delta}}} + \left( \frac{\gamma \bar{k} \sin(2\omega T_1)}{y_1^{\widehat{\delta}}} \right)^2 - \left( \frac{\gamma \bar{k} \sin(2\omega T_1)}{y_1^{\widehat{\delta}}} \right)^3 + \dots \right].$$

Using  $\delta = (\widehat{\delta})^2$  the factor on the left is:

$$\left( y_1^{\widehat{\delta}} + \gamma \bar{k} \sin(2\omega T_1) \right)^{\widehat{\delta}} = y_1^{\delta} + \gamma \frac{\widehat{\delta} y_1^{\delta}}{y_1^{\widehat{\delta}}} \bar{k} \sin(2\omega T_1) + O(\gamma^2).$$

Thus, truncating to order 1 in  $\gamma$ ,

$$\begin{aligned} \Phi_{\mathbf{w}}(\Phi_{\mathbf{v}})|_2 &= y_1^{\delta} + \gamma \frac{\widehat{\delta} y_1^{\delta}}{y_1^{\widehat{\delta}}} \bar{k} \sin(2\omega T_1) + \gamma \frac{K_1 \widehat{\delta}}{y_1^{\widehat{\delta}}} y_1^{\delta} \\ &= y_1^{\delta} + \gamma \frac{\widehat{\delta} y_1^{\delta}}{y_1^{\widehat{\delta}}} [K_1 + \bar{k} \sin(2\omega T_1)] + \dots \end{aligned}$$

and hence, taking  $y_1^{\delta}/y_1^{\widehat{\delta}} \approx 1$ , truncating the third component to order 0 in  $\gamma$ , and replacing  $y_1, z_1$  by  $y, z$  to lighten notation, the simplified version becomes:

$$\widetilde{G}(s, y, z) = \left( s + \frac{2 \ln \varepsilon}{\alpha + \beta} - \frac{(1 + \widehat{\delta}) \ln y}{\alpha + \beta}, y^{\frac{(\alpha - \beta)^2}{(\alpha + \beta)^2}} + \gamma (k_2 + k_1 \sin(2\omega s)), C_2 z y^{\frac{4\alpha}{(\alpha + \beta)^2}} \right) = (s, y, z)$$

where  $s$  is computed (mod  $\pi/\omega$ ) and we may take the constant  $k_2 = 1$  by rescaling  $\gamma$  with  $k_1 = \frac{\bar{k}}{K_1}$ . From now on we assume  $0 < k_1 \neq 1$  (see discussion of  $K_1$  in the beginning of this section).

**Remark 6.** For  $s = \gamma = 0$ ,  $\varepsilon = 1$ , is easy to check that the last two coordinates of  $\widetilde{G}$  coincide with  $G_0(y, z)$  in (3.7) and that the first coordinate equals the estimated time of first return  $T_1 + T_2$  given at the end of § 3.6.

**4.6. Reduction.** In the region  $(\alpha - \beta)^2 < 4\alpha$  for  $\alpha > 0$ ,  $\beta < 0$  (see Figure 4) the exponent of  $y$  in the second coordinate of  $\widetilde{G}(s, y, z)$  is smaller than in the third coordinate. Moreover, the first two coordinates do not depend on  $z$ . Hence, for small  $y$  we can ignore the last coordinate of  $\widetilde{G}$  and analyse the map, given in coordinates  $(s, y)$  by:

$$(4.14) \quad G_{\gamma}(s, y) = \left( s + \frac{2 \ln \varepsilon}{\alpha + \beta} - \frac{2\alpha}{(\alpha + \beta)^2} \ln y, y^{\delta} + \gamma (1 + k_1 \sin(2\omega s)) \right) = (g_1(s, y), g_2(s, y)).$$

We have also ignored terms that are  $O(\gamma^2)$  or higher, hence, for  $\gamma$  sufficiently small we have proved that if  $\gamma > 0$ ,  $\varepsilon = 1$  and  $(\alpha - \beta)^2 < 4\alpha$ , the first return map  $G$  to  $In(\mathbf{v})$  of the flow defined by (2.1) is approximated by the map:

$$G(s, y) = \left( s - \frac{2\alpha}{(\alpha + \beta)^2} \ln y, y^{\delta} + \gamma (1 + k_1 \sin(2\omega s)) \right) = (g_1(s, y), g_2(s, y)).$$

Theorem 1 is proved for the cross-section  $In(\mathbf{v})$ .

Although the map  $G$  only provides information about the flow of (2.1) if we take  $\gamma$  sufficiently small, the dynamics of (4.8) is worth studying in all cases, so we lift this restriction in later sections.

Recall that, as remarked in § 2.3 the natural phase space for (4.8) is the cylinder  $\mathcal{C}$  defined in (2.2).

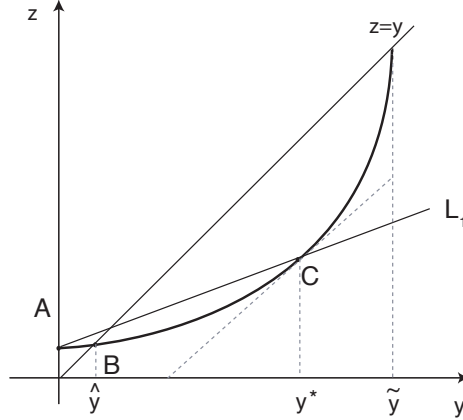


FIGURE 6. For  $k_1 = 0$  the second coordinate of the map  $G$  only depends on  $y$  and, under the conditions of Lemma 4, its graph has the shape of the curve above: it is convex near the origin and the point  $C$  where  $\mathbf{g}'(y) = 1$  lies below the diagonal  $z = y$ .

## 5. THE MAXIMAL ATTRACTOR

In this section, we obtain a flow-invariant subset of phase space by applying a general criterion called the Annulus Principle [4] – see also [28, § 4].

**5.1. The time averaged case.** We start by obtaining information on the map  $g_2$  in the special case  $k_1 = 0$ , when  $g_2(s, y) = y^\delta + \gamma =: \mathbf{g}(y)$ , where  $\delta = (\alpha - \beta)^2 / (\alpha + \beta)^2 > 1$ . In this case  $\mathbf{g}$  only depends on  $y$  and not on  $s$  and it may be seen as a time averaged simplification of the original  $g_2$ , analogous to the time averages of the Van der Pol method discussed in [1, Ch IX]. Let  $y_* = \delta^{\frac{1}{1-\delta}}$ .

**Lemma 4.** *If  $\delta > 1$  and  $0 < \gamma < \delta^{\frac{1}{1-\delta}} - \delta^{\frac{\delta}{1-\delta}} = M < 1$ , then:*

- (1) *near  $y = 0$  the map  $\mathbf{g}(y) = y^\delta + \gamma$  has a pair of fixed points  $0 < \hat{y} < \tilde{y}$ , that are respectively stable and unstable;*
- (2)  *$0 < \gamma < \hat{y} < y_* = \delta^{\frac{1}{1-\delta}}$  and  $0 < \hat{y} < \frac{\gamma\delta}{\delta-1}$ .*
- (3)  *$\tilde{y} > \gamma + \delta^{\frac{\delta}{1-\delta}} = \mathbf{g}(y_*)$ ;*

*Proof.* The result follows from the analysis of the graph of  $\mathbf{g}$ , shown in Figure 6. Specifically:

- (1) For small  $y \geq 0$ , we have :
  - $\mathbf{g}$  is convex in the neighbourhood of  $y = 0$ ;
  - $\mathbf{g}(0) = \gamma > 0$ ;
  - $\mathbf{g}'(y) = 1$  if and only if  $y_* := \delta^{\frac{1}{1-\delta}}$ ;
  - $\mathbf{g}(y_*) = \delta^{\frac{\delta}{1-\delta}} + \gamma < y_*$  if and only if the estimate of  $\gamma$  in the hypothesis holds.
 Hence, the point where the graph has slope 1 lies below the diagonal, and thus the graph of  $\mathbf{g}$  intersects the diagonal twice for small  $y > 0$ . At the first intersection  $\mathbf{g}'(\hat{y}) < 1$  hence  $\hat{y}$  is stable, whereas  $\mathbf{g}'(\tilde{y}) > 1$  hence  $\tilde{y}$  is unstable.
- (2) The first assertion, that  $0 < \gamma < \hat{y} < y_*$ , has already been established above. Let  $L_1$  be the line containing the two points  $A = (0, \gamma)$  and  $C = (y_*, \mathbf{g}(y_*))$ . Then the segment  $[AC]$  lies above the convex graph of  $\mathbf{g}$ . Since  $L_1$  intersects the diagonal at the point  $B$  with first coordinate  $\frac{\gamma\delta}{\delta-1}$ , then this number is an upper bound for  $\hat{y}$ .
- (3) Since  $\tilde{y} > y_*$ , then we also have  $\tilde{y} > \mathbf{g}(y_*) = \delta^{\frac{\delta}{1-\delta}} + \gamma$ , see Figure 6.

□

**5.2. The invariant annulus.** In this section we establish the existence of an annulus in the cylinder  $\mathcal{C} = \{(s, y) : y > 0, s \in \mathbf{R} \pmod{\pi/\omega}\}$  that is  $G$ -invariant. For this, as in § 5.1 above, let  $\hat{y}$  be the smallest (stable) positive solution of  $y = y^\delta + \gamma$  and let  $y_* = \delta^{1/(1-\delta)}$ . Since  $\delta > 1$  we have

$$(5.15) \quad \hat{y} > \gamma, \quad \text{and} \quad \delta \hat{y}^{\delta-1} < \delta (y_*)^{\delta-1} = 1.$$

Let  $R = \frac{2k_1}{1 - \delta \hat{y}^{\delta-1}} > 0$  and consider the annular region in the cylinder  $\mathcal{C}$  defined as:

$$\mathcal{A} = \{(s, y) : \hat{y} - R\gamma \leq y \leq \hat{y} + R\gamma \quad \text{and} \quad y > 0, \quad s \in \mathbf{R} \pmod{\pi/\omega}\},$$

whose interior is denoted  $\overset{\circ}{\mathcal{A}}$ . Note that the condition  $2k_1\gamma < \hat{y} - \delta \hat{y}^\delta$  is equivalent to:

$$\hat{y} - R\gamma = \hat{y} - \frac{2k_1\gamma}{1 - \delta \hat{y}^{\delta-1}} > \hat{y} - \frac{\hat{y} - \delta \hat{y}^\delta}{1 - \delta \hat{y}^{\delta-1}} = \hat{y} - \frac{\hat{y}(1 - \delta \hat{y}^{\delta-1})}{1 - \delta \hat{y}^{\delta-1}} = 0,$$

and the condition  $y > 0$  in the definition of  $\mathcal{A}$  is automatically fulfilled.

**Lemma 5.** *If  $\delta > 1$  and  $0 < \gamma < \delta^{\frac{1}{1-\delta}} - \delta^{\frac{\delta}{1-\delta}} = M < 1$ , then,  $G(\mathcal{A}) \subset \overset{\circ}{\mathcal{A}}$ , up to terms of order 2 in  $\gamma$ .*

*Proof.* By definition of  $\mathcal{A}$ , if  $(s, y) \in \mathcal{A}$  then  $0 < y \leq \hat{y} + R\gamma$ . Hence:

$$\begin{aligned} g_2(s, y) &= y^\delta + \gamma(1 + k_1 \sin(2\omega s)) = \mathbf{g}(y) + \gamma k_1 \sin(2\omega s) \\ &\leq (\hat{y} + R\gamma)^\delta + \gamma + \gamma k_1 \sin(2\omega s) \quad (\mathbf{g} \text{ is monotonically increasing}) \\ &= \hat{y}^\delta + R\gamma \delta \hat{y}^{\delta-1} + \gamma + \gamma k_1 \sin(2\omega s) + O(\gamma^2) \quad (\text{Taylor expansion in } \gamma) \\ &\leq \hat{y} + \gamma \left( R\delta \hat{y}^{\delta-1} + k_1 \right) + O(\gamma^2) \quad (\mathbf{g}(\hat{y}) = \hat{y} \text{ and majoration of } \sin) \\ &= \hat{y} + \gamma \left( R\delta \hat{y}^{\delta-1} + k_1 \frac{1 - \delta \hat{y}^{\delta-1}}{1 - \delta \hat{y}^{\delta-1}} \right) + O(\gamma^2) \\ &= \hat{y} + \gamma \left( \frac{2k_1 \delta \hat{y}^{\delta-1} + k_1 - k_1 \delta \hat{y}^{\delta-1}}{1 - \delta \hat{y}^{\delta-1}} \right) + O(\gamma^2) \quad (\text{replacing } R \text{ by its value}) \\ &< \hat{y} + \gamma \left( \frac{2k_1}{1 - \delta \hat{y}^{\delta-1}} \right) + O(\gamma^2) = \hat{y} + R\gamma + O(\gamma^2) \quad (\delta \hat{y}^{\delta-1} < 1). \end{aligned}$$

If  $\hat{y} - R\gamma < 0$  then the proof is complete. Otherwise, using  $y > \hat{y} - R\gamma$ , we may write

$$\begin{aligned} g_2(s, y) &= y^\delta + \gamma(1 + k_1 \sin(2\omega s)) = \mathbf{g}(y) + \gamma k_1 \sin(2\omega s) \\ &\geq (\hat{y} - R\gamma)^\delta + \gamma(1 + k_1 \sin(2\omega s)) \quad (\mathbf{g} \text{ is monotonically increasing}) \\ &= \hat{y}^\delta - R\gamma \delta \hat{y}^{\delta-1} + \gamma + \gamma k_1 \sin(2\omega s) + O(\gamma^2) \quad (\text{Taylor expansion in } \gamma) \\ &\geq \hat{y} - \gamma \left( R\delta \hat{y}^{\delta-1} - k_1 \right) + O(\gamma^2) \quad (\mathbf{g}(\hat{y}) = \hat{y} \text{ and minoration of } \sin) \\ &= \hat{y} - \gamma \left( \frac{2k_1}{1 - \delta \hat{y}^{\delta-1}} \delta \hat{y}^{\delta-1} - k_1 \frac{1 - \delta \hat{y}^{\delta-1}}{1 - \delta \hat{y}^{\delta-1}} \right) + O(\gamma^2) \quad (\text{replacing } R \text{ by its value}) \\ &= \hat{y} - \gamma \left( \frac{2k_1 \delta \hat{y}^{\delta-1} - k_1 + k_1 \delta \hat{y}^{\delta-1}}{1 - \delta \hat{y}^{\delta-1}} \right) + O(\gamma^2) \\ &> \hat{y} - \gamma \left( \frac{2k_1}{1 - \delta \hat{y}^{\delta-1}} \right) + O(\gamma^2) = \hat{y} - R\gamma + O(\gamma^2) \quad (\delta \hat{y}^{\delta-1} < 1) \end{aligned}$$

completing the proof. □

In particular, if  $O(\gamma^2)$  is negligible, then  $\mathcal{A}$  is  $G$ -invariant.

**5.3. Application of the annulus principle.** We recall the annulus principle (version [4]), adapted to our purposes:

**Theorem 6** (Prop. 1.4.6 in [4]). *Let  $G(\theta, y) = (\theta + g_1(\theta, y), g_2(\theta, y))$  be a diffeomorphism, with  $\theta \in \mathbf{R} \pmod{2\pi}$ , defined in the annulus  $\mathcal{B} = \{(\theta, y) : a \leq y \leq b \text{ and } \theta \in \mathbf{R} \pmod{2\pi}\}$ , where  $a < b$ , and satisfying:*

- (1)  $g_1$  and  $g_2$  are  $2\pi$ -periodic in  $\theta$  and smooth;
- (2)  $G(\mathcal{B}) \subset \overset{\circ}{\mathcal{B}}$ ;
- (3)  $\left|1 + \frac{\partial g_1}{\partial \theta}\right| > 0$ ;
- (4)  $\left|\frac{\partial g_2}{\partial y}\right| < 1$  (ie, the map  $g_2$  is a contraction in  $y$ );
- (5)  $2\sqrt{\left|\frac{\partial g_1}{\partial y}\right| \left|\frac{\partial g_2}{\partial \theta}\right|} < \left|1 + \frac{\partial g_1}{\partial \theta}\right| - \left|\frac{\partial g_2}{\partial y}\right|$ ;
- (6)  $\left|1 + \frac{\partial g_1}{\partial \theta}\right| + \left|\frac{\partial g_2}{\partial y}\right| < 2$ .

then the maximal attractor in  $\mathcal{B}$  is an invariant closed curve, the graph of a  $2\pi$ -periodic,  $C^1$  function  $y = h(\theta)$ .

For  $|y - \hat{y}| \leq R\gamma$ , let  $\Psi(y) = y^{1/2} - \delta y^{\delta-1/2}$ . This expression is well defined, since we have shown above that  $\hat{y} - R\gamma > 0$ .

**Theorem 7.** *For  $\delta > 1$ , if  $0 < \gamma < \delta^{\frac{1}{1-\delta}} - \delta^{\frac{\delta}{1-\delta}} = M < 1$  and if  $\Psi(y)$  satisfies  $\Psi(\hat{y} - R\gamma) > Z$  and  $\Psi(\hat{y} + R\gamma) > Z$  for  $Z = 4\sqrt{\omega\alpha\gamma k_1}/(\alpha + \beta)$ , then the maximal attractor in  $\mathcal{A}$  is an invariant closed curve, the graph of a  $\pi/\omega$ -periodic,  $C^1$  function  $y = h(s)$ .*

*Proof.* This is an application of Theorem 6. In order to be in the conditions of Theorem 6 we replace in  $G(s, y)$  the variable  $s$  by  $\theta = 2\omega s$ . Hence, we get:

$$g_1(\theta, y) = -K_* \ln y \quad \text{and} \quad g_2(\theta, y) = y^\delta + \gamma(1 + k_1 \sin \theta) \quad \text{where} \quad K_* = \frac{4\omega\alpha}{(\alpha + \beta)^2}$$

with derivatives

$$\frac{\partial g_1}{\partial \theta} = 0 \quad \frac{\partial g_1}{\partial y} = -\frac{K_*}{y} \quad \frac{\partial g_2}{\partial \theta} = \gamma k_1 \cos \theta \quad \frac{\partial g_2}{\partial y} = \delta y^{\delta-1}.$$

Conditions (1) and (3) are immediate, (2) follows by Lemma 5 and (4) from (5.15). For (6) note that  $\left|\left(1 + \frac{\partial g_1}{\partial \theta}\right)\right| + \left|\frac{\partial g_2}{\partial y}\right| = 1 + \left|\frac{\partial g_2}{\partial y}\right| \leq 1 < 2$  because  $\delta y^{\delta-1} < 1$  by (3) of Lemma 4.

Finally, for (5), we want to show that  $2\sqrt{\left|\frac{\partial g_1}{\partial y}\right| \left|\frac{\partial g_2}{\partial \theta}\right|} < \left|1 + \frac{\partial g_1}{\partial \theta}\right| - \left|\frac{\partial g_2}{\partial y}\right|$ . Observe that:

$$2\sqrt{\left|\frac{\partial g_1}{\partial y}\right| \left|\frac{\partial g_2}{\partial \theta}\right|} = 2\sqrt{\left|\frac{K_*}{y}\right| \cdot |\gamma k_1 \cos \theta|} \quad \text{and that} \quad \left|1 + \frac{\partial g_1}{\partial \theta}\right| - \left|\frac{\partial g_2}{\partial y}\right| = 1 - |\delta y^{\delta-1}|.$$

Since we want (5) to hold for all  $\theta$  and since  $y > 0$ , we want to prove that

$$2\sqrt{\frac{K_*\gamma k_1}{y}} < 1 - \delta y^{\delta-1},$$

or, equivalently, that  $\Psi(y) > 2\sqrt{K_*\gamma k_1} = Z$ . Since  $\Psi(y)$  has only one critical point for  $y > 0$ , a maximum at  $y = (2\delta(\delta - 1/2))^{\frac{1}{1-\delta}}$ , the hypothesis that  $\Psi(y) > Z$  at the two endpoints of the interval  $|y - \hat{y}| \leq R\gamma$  is sufficient to guarantee that (5) holds.  $\square$

The condition  $\Psi(\hat{y} \pm R\gamma) \geq 4\sqrt{\omega\alpha\gamma k_1}/(\alpha + \beta)$  in Theorem 7 is not unreasonable. For instance, if we fix  $\gamma$ ,  $k_1$ ,  $\alpha$  and  $\beta$  then  $\delta$ ,  $\hat{y}$  and  $R$  are defined and fixed. In this case for  $\omega$  small enough the condition is fulfilled. This condition plays the same role as the condition  $0 < a < \frac{1}{\sqrt{1 + \eta^2}}$  in Theorem 3.2 of [3].

Since the invariant curve of Theorem 7 is the graph of a function  $y = h(s)$  it follows that it is not contractible on the cylinder, as claimed in the statement of Theorem B.

## 6. FINDING PERIODIC SOLUTIONS: STABILITY AND BIFURCATIONS

In this section, we study periodic solutions to (2.1) and their period. We also discuss their bifurcations when the parameters  $\gamma$  and  $k_1$  vary. We introduce an auxiliary parameter  $T$ , and in § 6.2, § 6.3 and § 6.4 we analyse the bifurcations on this parameter for different values of  $\gamma > 0$  and  $k_1 > 0$ . The auxiliary parameter  $T$  is then removed in § 6.5 to yield solutions of the original problem.

We address the problem of solving the equation  $\mathcal{G}_T(s, y) = G(s, y) - (T, 0) = (s, y)$  for the first return map. This means that we need to solve:

$$(6.16) \quad \mathcal{G}_T(s, y) = \left( s - \frac{\ln y}{K}, y^\delta + \gamma(1 + k_1 \sin(2\omega s)) \right) - (T, 0) = (s, y)$$

for  $T > 0$ , the fixed points of  $\mathcal{G}_T(s, y)$ .

**6.1. The time averaged case.** In the special case  $k_1 = 0$  the perturbation is autonomous and we have:

**Lemma 8.** *Suppose  $k_1 = 0$ . For  $\gamma > 0$  small, there are two fixed points of  $\mathcal{G}_T(s, y)$ , one stable and the other unstable, with the value of  $T$  tending to  $+\infty$  when  $\gamma$  tends to 0. When  $\gamma$  reaches a threshold value  $M$ , the two fixed points collapse at a saddle-node bifurcation and for  $\gamma > M$  there are no fixed points of  $\mathcal{G}_T(s, y)$ .*

*Proof.* Solving the first component of (6.16) we get  $y = e^{-KT}$ . For the second coordinate we get  $\gamma = y - y^\delta$ , replacing  $y$  by  $e^{-KT}$  in this expression we obtain

$$F(T) = e^{-KT} - e^{-\delta KT}.$$

The result will follow directly from the properties of the graph of  $F(T)$ , shown in Figure 7, that we state as a separate lemma for future use.  $\square$

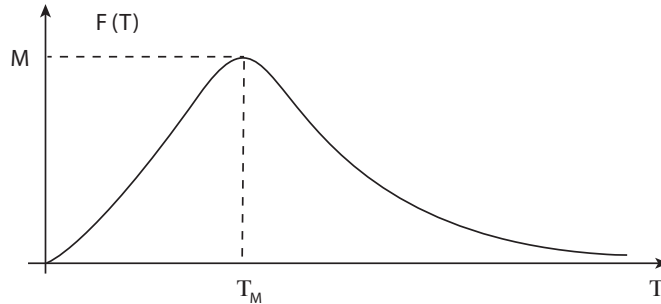


FIGURE 7. The graph of  $F(T) = e^{-KT} - e^{-\delta KT}$ , that attains its maximum at  $T_M = \frac{\ln \delta}{K(\delta - 1)} > 0$ .

**Lemma 9.** *The map  $F(T) : \mathbf{R}^+ \rightarrow [0, 1]$  has a global maximum  $M$  at  $T_M = \frac{\ln \delta}{K(\delta - 1)} > 0$  and*

$$\lim_{T \rightarrow 0} F(T) = \lim_{T \rightarrow \infty} F(T) = 0.$$

*Proof.* Differentiating  $F$  with respect to  $T$ , we get:

$$(6.17) \quad \frac{dF}{dT}(T) = -Ke^{-TK} + \delta Ke^{-\delta TK} = -Ke^{-TK} \left(1 - \delta e^{-(\delta-1)TK}\right).$$

From this it is immediate that  $\frac{dF}{dT}(T) = 0$  precisely at  $T = T_M$ , that  $\frac{dF}{dT}(T) > 0$  for  $T < T_M$  and  $\frac{dF}{dT}(T) < 0$  for  $T > T_M$ . Finally, we compute

$$(6.18) \quad M = F(T_M) = \delta^{\frac{1}{1-\delta}} - \delta^{\frac{\delta}{1-\delta}} > 0.$$

The two limits are immediate from the expression for  $F(T)$ . Note that  $M < 1$  because  $\delta - \delta^\delta < 0 < \delta^{1-\delta}$ , hence  $F(T) < 1$ . Finally  $F(T) > 0$  because  $e^{KT} < e^{\delta KT}$ .  $\square$

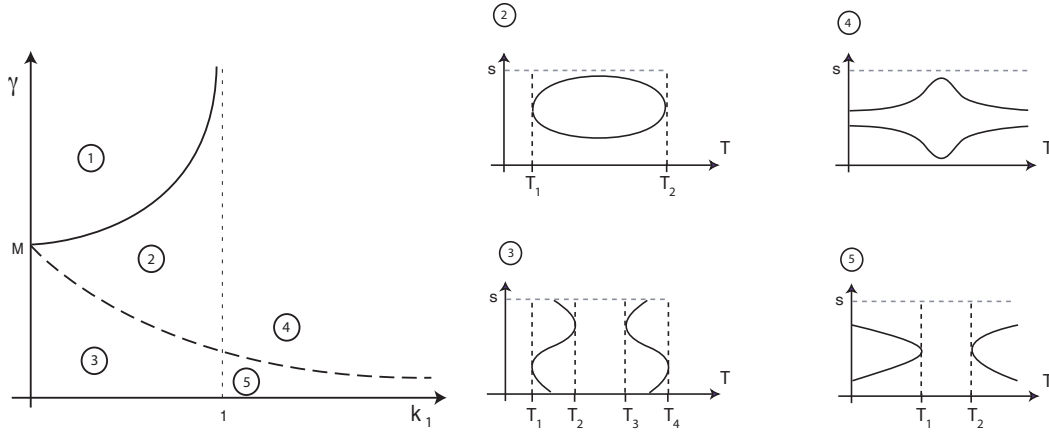


FIGURE 8. Left: bifurcation diagram on  $(k_1, \gamma)$ -plane for the solutions of (6.16): the solid line is  $\gamma = M/(1-k_1)$ , the dashed line is  $\gamma = M/(1+k_1)$ . Numbering corresponds to Proposition 10. In region (1) there are no solutions. The geometry of the solution set for parameters in the other four open regions is show on the right. Recall that the variable  $s$  is cyclic, so the solutions lie on the surface of a cylinder parametrised by  $s \in [0, 2\pi/\omega]$  and that  $y = e^{-KT}$ .

**6.2. First result.** The key result in the analysis is the bifurcation diagram for  $\mathcal{G}_T(s, y)$ , shown in Figure 8 and described in the next proposition:

**Proposition 10.** For  $k_1 > 0$ ,  $\gamma > 0$ , fixed points of  $\mathcal{G}_T(s, y)$ , solutions of (6.16) with  $T > 0$ , satisfy

$$(6.19) \quad y(T) = e^{-KT}.$$

For  $M = \delta^{\frac{1}{1-\delta}} - \delta^{\frac{\delta}{1-\delta}} > 0$ , the curves  $k_1 = 1$  and  $\gamma(1-k_1) = M$  and  $\gamma(1+k_1) = M$  separate the first quadrant of the  $(k_1, \gamma)$ -plane into five regions (see Figure 8) with the following behaviour:

- (1)  $k_1 \in (0, 1)$  and  $M < \gamma(1-k_1)$  — there are no fixed points;
- (2)  $k_1 \in (0, 1)$  and  $\gamma(1-k_1) < M < \gamma(1+k_1)$  — there are fixed points for each  $T \in [T_1, T_2]$ ;
- (3)  $k_1 \in (0, 1)$  and  $\gamma(1+k_1) < M$  — there are fixed points for each  $T \in [T_1, T_2] \cup [T_3, T_4]$ ;
- (4)  $k_1 > 1$  and  $M < \gamma(1+k_1)$  — there are fixed points for each  $T \in \mathbf{R}^+$ ;
- (5)  $k_1 > 1$  and  $\gamma(1+k_1) < M$  — there are fixed points for each  $T \in (0, T_1] \cup [T_2, \infty)$ ;

where  $0 < T_1 < T_2 < T_3 < T_4$ . Moreover, when fixed points exist for  $T$  in an interval, then there are two fixed points  $(s, y)$  and  $(s', y)$  for each  $T$  in the interior of the interval and only one for  $T$  in the boundary. These qualitative features occur for every  $\omega > 0$  and only the initial time  $s$  depends on  $\omega$ .

*Proof.* Solving the first component of (6.16) we get  $y$  as a function of  $T \in \mathbf{R}^+$  as in (6.19). The map  $y : \mathbf{R}^+ \rightarrow \mathbf{R}^+$  satisfies the following properties:

- $\lim_{T \rightarrow 0} y(T) = 1$

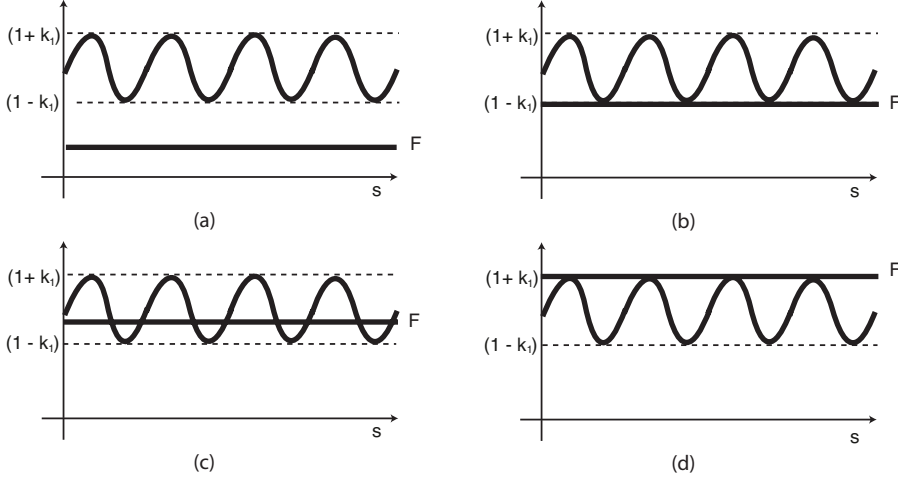


FIGURE 9. For each value of the frequency  $\omega$ , the solution of  $F(T) = \phi_\omega(s)$  lies on the intersection of the graph of  $\Phi_\omega$  with a horizontal line at height  $F(T)$ . As  $T$  increases the horizontal line moves up, until it reaches its maximum height  $M$ . After this the height decreases to zero. Here is illustrated the case  $0 < k_1 < 1$  and  $\gamma < M/(1 + k_1)$ , for  $F(T)$  increasing from (a) to (d).

- $\lim_{T \rightarrow +\infty} y(T) = 0$  and
- $y$  decreases monotonically with  $T$ .

From the second coordinate of (6.16) we have that  $y$  must also satisfy  $y^\delta + \gamma(1 + k_1 \sin(2\omega s)) = y$ , which is equivalent to:

$$(6.20) \quad y - y^\delta = \gamma(1 + k_1 \sin(2\omega s)).$$

The left hand side of (6.20) does not depend on  $s$  nor on  $\omega$ . Replacing  $y$  by the expression (6.19) yields the map  $F$  that was analysed in Lemma 9.

In order to find the fixed points of  $\mathcal{G}_T(s, y)$ , solutions of (6.16), we need to solve for  $s$  the expression  $F(T) = \phi_\omega(s)$  where

$$\phi_\omega(s) = \gamma(1 + k_1 \sin(2\omega s)).$$

This amounts to intersecting the graph of  $\phi_\omega(s)$  with a horizontal line because  $F(T)$  does not depend on  $s$ . The line moves first up and then down as  $T$  increases, as in Figure 9. Since the range of  $\phi_\omega$  is the interval  $[\gamma(1 - k_1), \gamma(1 + k_1)]$ , and the range of  $F(T)$  is the interval  $(0, M]$ , the geometry of the solution set depends on the relative positions of these intervals. The persistent possibilities are shown in Figure 10. The possibilities correspond to cases (1) – (5), shown in Figure 8.

Case (1) is the simplest: if  $M < \gamma(1 - k_1)$  then the maximum  $M$  of  $F(T)$  never reaches the minimum value of  $\phi_\omega$ , as in Figure 9 (a). This implies that there are no fixed points of  $\mathcal{G}_T$  for any  $T$ . This is only possible if  $k_1 \in (0, 1)$ , since  $M > 0$ . For all other cases, there are intervals of  $T$  values where (6.16) has a solution  $(s, y(T))$ , with  $y(T) = e^{-KT}$  and  $s \in [0, \pi/\omega]$ , so the true representation of the solutions should be a  $T$ -parametrised curve on a cylinder.

Still with  $k_1 \in (0, 1)$ , for  $\gamma$  smaller than in case (1) we have cases (2) and (3). As  $T$  increases from 0, there is a threshold value  $T_1$  for which the horizontal line at height  $F(T)$  first touches the graph of  $\phi_\omega$  as in Figure 9 (b). At these points we have  $\sin(2\omega s) = -1$ . As  $T$  increases further, each tangency point unfolds as two intersections of the graph with the horizontal line as in Figure 9 (c). Thus, there is a saddle-node at the points

$$(s_N, y(T_1)) = \left( \frac{3\pi}{4\omega}, y(T_1) \right).$$

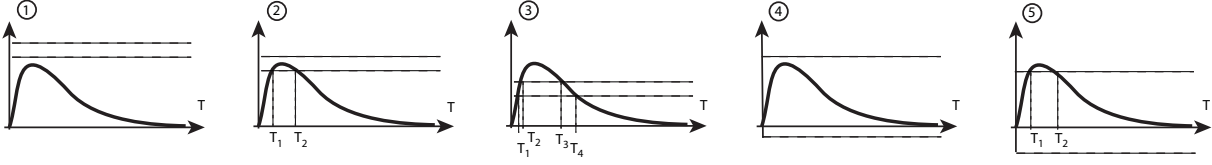


FIGURE 10. Persistent possibilities for the relative position of the graph of  $F(T)$  and the (dashed) horizontal lines at heights  $\gamma(1 - k_1)$  and  $\gamma(1 + k_1)$  that delimit the range of  $\phi_\omega(s)$ . The numbering corresponds to the cases in Proposition 10.

In case (2) when the maximum  $M$  of  $F(T)$  is attained, the horizontal line is still in the middle of the graph of  $\phi_\omega$  as Figure 9 (c), so the two solutions coalesce at a second saddle-node at  $(s_N, y(T_2)) = (3\pi/4\omega, y(T_2))$ . In case (3) the horizontal line may move further up as in Figure 9 (d) and a pair of solutions come together at a second saddle-node at  $(s_N, y(T_2)) = (\pi/4\omega, y(T_2))$  and reappear at a saddle-node at  $(s_N, y(T_3)) = (\pi/4\omega, y(T_3))$  coming together finally at  $(s_N, y(T_4)) = (3\pi/4\omega, y(T_4))$ . We show below that at these points the derivative  $D\mathcal{G}_T(s, y)$  has an eigenvalue equal to 1.

Finally for cases (4) and (5), the minimum value of  $\phi_\omega(s)$  is negative, hence for both small and very large values of  $T$  the horizontal line at height  $F(T)$  always crosses the graph of  $\phi_\omega(s)$ . In case (4) this is all that happens and there are solutions for all values of  $T > 0$ . In case (5) the horizontal line moves above the graph of  $\phi_\omega(s)$  and thus there is an interval  $(T_1, T_2)$  of periods for which there are no solutions, with end points at two saddle-nodes as above.  $\square$

Note that in Proposition 10 the values of  $y$  and  $T$  for which solutions of (6.16) exist do not depend on the frequency  $\omega$ , and only the initial time  $s$  does. All the solutions satisfy  $y \in [0, 1]$  because this interval is the range of the map  $y(T)$ . This is compatible with the assumption made in § 3.2 that  $y \leq \varepsilon$ , and the fact that in (4.8) we have set  $\varepsilon = 1$ .

From the proof of Proposition 10 it follows:

**Corollary 11.** *For  $k_1 > 0$ ,  $\gamma > 0$ ,  $\gamma = M/(1 \pm k_1)$ , fixed points of  $\mathcal{G}_T(s, y)$ , solutions of (6.16), with  $T > 0$  undergo saddle-node bifurcations at points  $T_j$  satisfying*

$$F(T_j) = \gamma(1 + k_1) \quad \forall k_1 \quad \text{and if } k_1 > 1 \text{ then also } F(T_j) = \gamma(1 - k_1).$$

*Thus these points define surfaces in the 3-dimensional parameter space  $(T, k_1, \gamma)$ . For  $(k_1, \gamma)$  in regions (2) and (5) of Theorem 12, there are saddle-node bifurcations at two values of  $T$ , whereas in region (3) they occur at four values of  $T$ .*

**6.3. Bifurcations.** The organising centres for all the local dynamics are the most degenerate points on the bifurcation diagram of Proposition 10. They are points where solutions of (6.16) undergo a discrete-time Bogdanov-Takens bifurcation, that was studied in [7, 33], see also [2, Ch 2 §2]. These points are characterised by the eigenvalues of the derivative of  $\mathcal{G}_T$ .

**Theorem 12.** *For  $\gamma = M/(1 \pm k_1)$  and  $T = T_M$ , the derivative  $D\mathcal{G}_T(s, y)$  at a solution of (6.16) has 1 as a double eigenvalue and is not the identity. Moreover, these are the only points where  $D\mathcal{G}_T(s, y)$  has a double eigenvalue 1.*

*Proof.* We compute the derivative  $D\mathcal{G}_T(s, y)$  at the points  $(s_N, y(T_N))$ ,  $N = 1, \dots, 4$ , where  $\sin(2\omega s_N) = \pm 1$  and get:

$$D\mathcal{G}_T(s_N, y(T_N)) = \begin{pmatrix} 1 & -\frac{1}{Ky} \\ 0 & \delta y^{\delta-1} \end{pmatrix}.$$

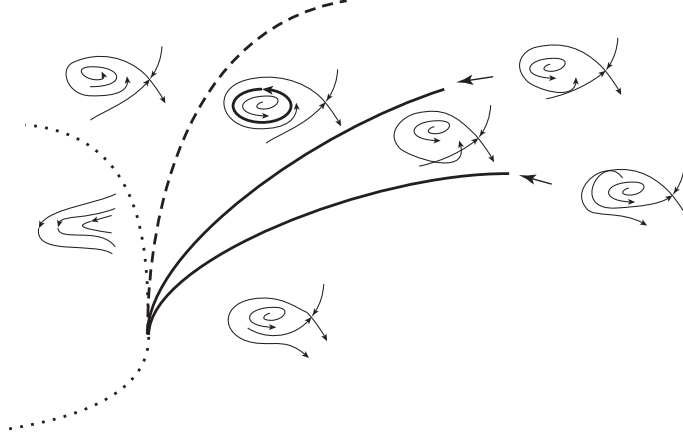


FIGURE 11. Bifurcation diagram for the discrete-time Bogdanov-Takens bifurcation [7, 33]. Conventions: saddle-nodes on the dotted line, Hopf bifurcation on the dashed line, homoclinic tangencies (shown on the right) on the solid lines. A closed invariant curve exists for parameters between the line of Hopf bifurcation and the line of homoclinic tangency. The position of the two solid lines in the figure is grossly exaggerated, the two curves have an infinite order tangency at the bifurcation point.

At  $(s_N, y(T_N))$  the Jacobian matrix is triangular and so the two eigenvalues are  $\mu_1 = 1$  and  $\mu_2 = \delta y^{\delta-1} > 0$ . Using (6.19) this may be rewritten as  $\mu_2 = \delta e^{-(\delta-1)T_N K}$ . Since  $T_M$  was defined to be the value of  $T$  where the function  $F(T)$  has a global maximum, then  $\frac{dA}{dT}(T_M) = 0$ . By (6.17) this means

$$1 = \delta e^{-(\delta-1)T_M K} = \delta (y(T_M))^{\delta-1} = \mu_2.$$

Hence the derivative of  $\mathcal{G}_T$  at these points has a double eigenvalue equal to 1, and is not the identity. The points in question are those where  $\sin(2\omega s_N) = \pm 1$  for  $(s_N, y(T_N))$ , hence  $F(T_N) = \gamma(1 \pm k_1)$  and  $T_N = T_M$  implying  $F(T_M) = M = \gamma(1 \pm k_1)$ .

Finally,  $D\mathcal{G}_T(s, y)$  has a double eigenvalue 1 if and only if the trace  $\text{tr } D\mathcal{G}_T(s, y) = 2$  and  $\det D\mathcal{G}_T(s, y) = 1$ . Computing the Jacobian

$$D\mathcal{G}_T(s, y) = \begin{pmatrix} 1 & -\frac{1}{Ky} \\ 2\omega\gamma k_1 \cos(2\omega s) & \delta y^{\delta-1} \end{pmatrix}$$

then  $\text{tr } D\mathcal{G}_T(s, y) = 1$  implies that  $\delta y^{\delta-1} = 1$  and by (6.19) this means  $\delta e^{-(\delta-1)TK} = 1$ . Using (6.17) it follows that  $\frac{dA}{dT}(T) = 0$  hence  $T = T_M$ . On the other hand since  $\delta y^{\delta-1} = 1$ , then

$$\det D\mathcal{G}_T(s, y) = 1 + 2\omega\gamma k_1 \cos(2\omega s)/Ky.$$

Therefore,  $\det D\mathcal{G}_T(s, y) = 1$  implies  $\cos(2\omega s) = 0$ , hence  $\sin(2\omega s) = \pm 1$  and  $T = T_N$ ,  $N = 1, \dots, 4$ . The coincidence  $T_N = T_M$  only happens if  $\gamma = M/(1 \pm k_1)$ .  $\square$

The situation described in Theorem 12 occurs on the boundaries between the regions of Proposition 10. Geometrically what is happening is that two solution branches come together as in Figure 12. This indicates a bifurcation of codimension 2 — corresponding to a curve in the 3-dimensional parameter space  $(T, k_1, \gamma)$ , where we expect to find a discrete-time Bogdanov-Takens bifurcation, described in [7, 33] (see Figure 11). This bifurcation occurs at points where 1 is a double eigenvalue, where the derivative is not the identity and where the map also satisfies some more complicated non degeneracy conditions on the nonlinear part. Instead of verifying these additional conditions, we check that the linear conditions for nearby local bifurcations arise in a form consistent with the versal unfolding of

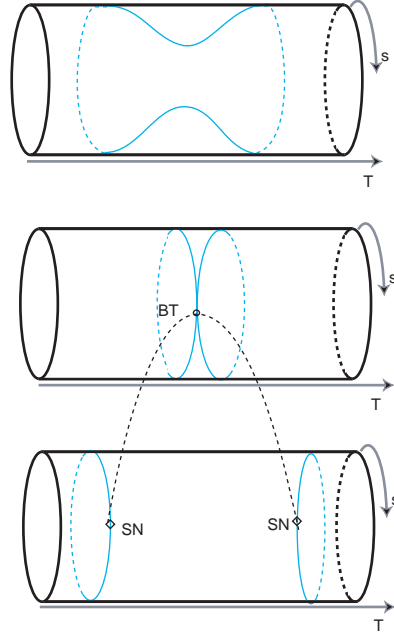


FIGURE 12. Bifurcation diagram of fixed points of  $\mathcal{G}_T(s, y)$  on the cylinder  $(T, s)$ , with  $s \in \mathbf{R} \pmod{\pi/\omega}$ , in the transition from case (2) to case (3) of Proposition 10. When  $\gamma$  increases, saddle-node bifurcation points SN come together at a point BT of discrete-time Bogdanov-Takens bifurcation [7, 33]. A line of Hopf bifurcation points also arises here, creating an invariant circle on the cylinder, and a region of chaotic dynamics appears further on.

the discrete-time Bogdanov-Takens bifurcation. Around this bifurcation, by the results of [7, 33], we expect to find the following codimension one bifurcations (see Figure 13):

- (a) a surface of saddle-node bifurcations;
- (b) a surface of Hopf bifurcations;
- (c) two surfaces of homoclinic tangencies.

The surfaces of saddle-node bifurcations in (a) have been described in Corollary 11. Numerical plots of these curves are shown in Figure 14 as curves in  $(T, \gamma)$  planes, for fixed values of  $k_1$ . The stability of bifurcating solutions is discussed below in § 6.4.

The points (b) of Hopf bifurcation in Figure 14 were determined numerically for fixed  $k_1$ , as a curve in the  $(T, \gamma)$  plane, using the conditions  $\text{tr } D\mathcal{G}_T(s, y) \in (-2, 2)$  and  $\det D\mathcal{G}_T(s, y) = 1$ . For the first condition, we use  $\text{tr } D\mathcal{G}_T(s, y) = \delta y^{\delta-1} + 1 > 0$  and since  $y = e^{-KT}$ , we get  $\text{tr } D\mathcal{G}_T(s, y) < 2$  if and only if  $T > \frac{\ln \delta}{K(\delta-1)}$ . The second condition expands to

$$K e^{-KT} \left( 1 - \delta e^{-K(\delta-1)T} \right) = 2\omega\gamma k_1 \cos 2\omega s$$

or, equivalently,

$$-\frac{dF(T)}{dt} = \frac{d\phi_\omega}{ds} \quad \text{and} \quad F(T) = \phi_\omega(s) = \gamma(1 + k_1 \sin 2\omega s).$$

Writing  $C = k_1 \cos 2\omega s = -\frac{dF(T)}{dt} \frac{1}{2\omega\gamma}$  we obtain  $k_1 \sin 2\omega s = \sqrt{k_1^2 - C^2}$  and hence

$$\frac{F(T)}{\gamma} - 1 = \sqrt{k_1^2 - \frac{1}{4\omega^2\gamma^2} \left( \frac{dF(T)}{dT} \right)^2}.$$

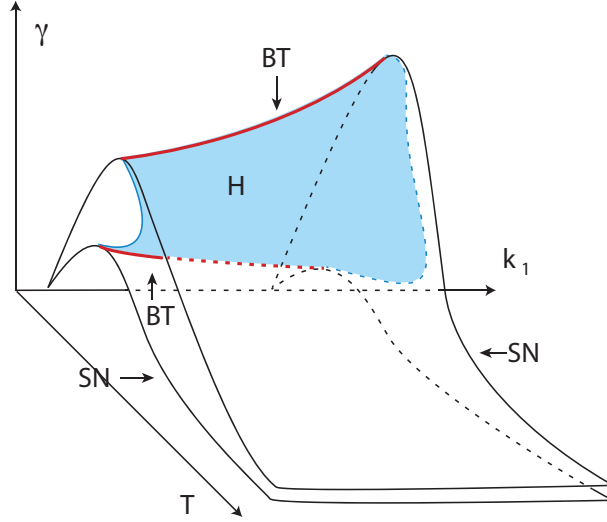


FIGURE 13. Schematic representation of the bifurcations of fixed points of  $\mathcal{G}_T(s, y)$  around the discrete-time Bogdanov-Takens, with  $k_1 < 1$ : the surfaces (a) of saddle-nodes SN (white) and the surface (b) of Hopf bifurcations H (blue) coming out of the red lines  $\gamma = M/(1 - k_1)$  and  $\gamma = M/(1 + k_1)$  of Bogdanov-Takens bifurcation points BT.

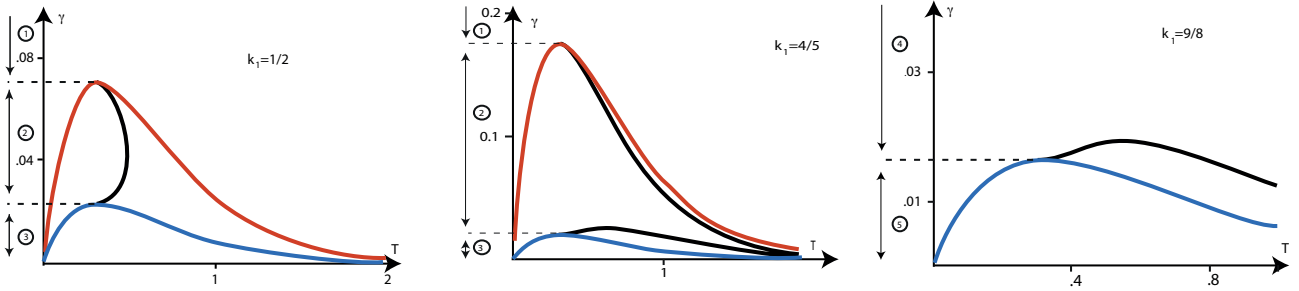


FIGURE 14. Numerical plot (using Maxima) of the lines of Hopf (black) and saddle-node (red and blue) bifurcation of fixed points of  $\mathcal{G}_T(s, y)$ , for different values of  $k_1$ . The lines of Hopf bifurcation terminate where they meet one of the lines of saddle-nodes, at a point of discrete-time Bogdanov-Takens bifurcation. Remaining parameters are  $K = 3$ ,  $\omega = 1$  and  $\delta = 1.1$ . Numbers inside circles near the  $\gamma$  axis indicate the region of Proposition 10 where  $(k_1, \gamma)$  lies.

This shows that  $D\mathcal{G}_T(s, y)$  has non real eigenvalues on the unit circle if and only if

$$T > T_M \quad \text{and} \quad (F(T) - \gamma)^2 - k_1^2 \gamma^2 + \frac{1}{4\omega^2} \left( \frac{dF(T)}{dT} \right)^2 = 0.$$

The two surfaces (c) correspond to bifurcations at which the stable and unstable manifolds of a saddle point are tangent. In the region between these surfaces there is a transverse intersection of the stable and the unstable manifolds of the saddle. In Figure 11, for simplicity, we only show one intersection of the stable and the unstable manifolds of the saddle, but these intersections are repeated at an orbit that accumulates on the saddle in forward and backward times. Around the transverse intersection of the manifolds, horseshoe dynamics occurs. The distance between the two bifurcation curves is exponentially small with respect to  $\sqrt{\|(k_1, \gamma)\|}$  and the invariant manifolds intersect inside the parameter region between the curves and do not intersect outside it. This configuration implies that the dynamics of  $G$  is equivalent to Smale's horseshoe.

**6.4. Stability of solutions.** A pair of fixed points of  $\mathcal{G}_T(s, y)$ , solutions of (6.16), bifurcate at the saddle-nodes of Corollary 11. We denote their first coordinate by  $s_* < s_\diamond$ . Taking  $s_*, s_\diamond \in [0, \pi/\omega]$ , this order completely identifies each solution.

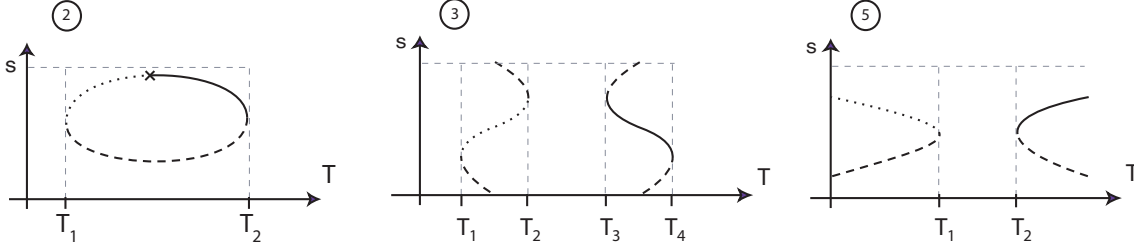


FIGURE 15. Schematic stability of fixed points of  $\mathcal{G}_T(s, y)$ , solutions of (6.16), in regions (2), (3) and (5) of Proposition 10. Conventions: solid lines are sinks, dashed lines are saddles, dotted lines are sources. Recall that  $y$  is a decreasing function of  $T$ . In region (2) the upper branch must undergo a bifurcation, indicated by an X, probably the Hopf bifurcation of Figure 14.

**Proposition 13.** *The solutions  $(s_*, y_*)$  and  $(s_\diamond, y_\diamond)$  with  $s_* < s_\diamond \in [0, \pi/\omega]$ , of (6.16) created at the saddle-nodes of Corollary 11 bifurcate with the following stability assignments (see Figure 15):*

region	(2)		(3)				(5)	
branch \ saddle-node	$T_1$	$T_2$	$T_1$	$T_2$	$T_3$	$T_4$	$T_1$	$T_2$
$s_\diamond$	source	sink	source	saddle	saddle	sink	source	sink
$s_*$	saddle	saddle	saddle	source	sink	saddle	saddle	saddle

*Proof.* The stability of solutions of (6.16) is obtained from the eigenvalues of the derivative  $D\mathcal{G}_T(s, y)$ . They are easier to compute at the saddle-node points  $(s_N, y(T_N))$ ,  $N = 1, \dots, 4$ , where they are  $\mu_1 = 1$  and  $\mu_2 = \delta y^{\delta-1} > 0$ , as in the beginning of the proof of Theorem 12.

In region (5) there are two saddle-node points at  $T_1 < T_M < T_2$ . At  $T_1$  we have  $\mu_2 > 1$ , so the solutions that bifurcate from this point are unstable. The eigenvalue is  $\mu_2 < 1$  at  $T_2$  and the stability of the bifurcating solutions is determined by the other eigenvalue,  $\mu_1$ . First note that the trace of the Jacobian  $\text{tr } D\mathcal{G}_T(s, y) = 1 + \delta y^{\delta-1} = \mu_1 + \mu_2$  does not depend on  $s$ , hence it has the same value on the two bifurcating branches. This is not true of the determinant of the Jacobian, given by

$$\det D\mathcal{G}_T(s, y) = \delta y^{\delta-1} + (\gamma k_1 \omega \cos(2\omega s)) / Ky = \mu_1 \mu_2.$$

On the other hand, the tangency of  $F(T_2)$  to the graph of  $\phi_\omega(s)$  occurs when  $\sin(2\omega s) = +1$  and thus around this point  $\cos(2\omega s)$  decreases with  $s$ . Therefore  $\det D\mathcal{G}_T(s, y)$  is smaller at  $(s_\diamond, y_\diamond)$  and these points are sinks whereas the points  $(s_*, y_*)$  are saddles. A similar reasoning shows that for the solutions with  $T < T_M$ , the points  $(s_\diamond, y_\diamond)$  are sources and  $(s_*, y_*)$  are saddles, as in Figure 15.

Applying the reasoning above to region (2) shows that at  $T_1$  the saddle-node bifurcation yields sources at  $s_\diamond$  and saddles at  $s_*$ . At  $T_2$  one would get of sinks at  $s_\diamond$  and saddles at  $s_*$ . Since there is only one top branch, there must be some additional bifurcation along it.

In region (3) there are four saddle-node points at  $T_1 < T_2 < T_M < T_3 < T_4$ , see Figure 15. The arguments used to discuss case (5) show that for  $T \in (T_3, T_4)$  there is a branch of sinks and a branch of saddles, whereas the branches with  $T \in (T_1, T_2)$  are of saddles and of sources. Note that branch of saddles  $(s_\diamond, y_\diamond)$  that bifurcates at  $T_3$  arrives at  $T_4$  as  $(s_*, y_*)$  by going around the cylinder (see Figure 15). The same happens at the branch of saddles that bifurcate at  $T_1$  and  $T_2$ .  $\square$

In region (4) there are no saddle-nodes, so it is more difficult to assign stabilities. In region (2) we expect a Hopf bifurcation to occur on the branch  $s_\diamond$ . The transition between regions (2) and (3) is a Bogdanov-Takens bifurcation where two saddle-node branches and Hopf bifurcation points come together at the same point.

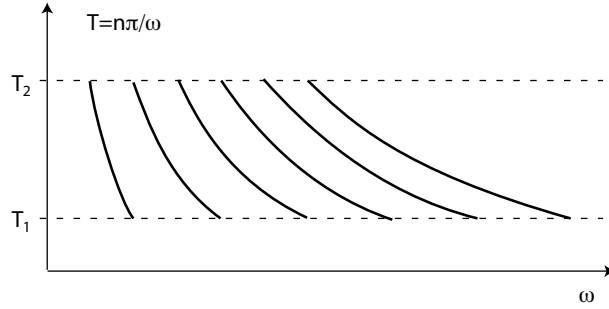


FIGURE 16. Periods of frequency locked solutions to (6.16) in region (2) of Proposition 10. For each point in one of the curves there are two periodic solutions of this period.

**6.5. Frequency locking.** The fixed points of  $\mathcal{G}_T(s, y)$ , solutions of (6.16), are fixed points of  $G$  in the cylinder whenever the point  $(s + T, y)$  coincides with  $(s, y)$  and this happens when  $T$  is an integer multiple of  $\pi/\omega$ . These points correspond to periodic solutions of the periodically forced equation (2.1) whose period is locked to the external forcing.

**Definition 1.** A periodic solution of a periodically forced differential equation is said to be frequency locked if its period is an integer multiple of the period of the external forcing.

We discuss here the frequency locked solutions of (6.16). Proposition 10 shows that if  $\gamma(1 - k_1) < M$  then for each forcing frequency  $\omega > 0$  there exist at least two branches of periodic solutions to (6.16). These branches are curves in  $(s, y, T)$ -space, each point in a curve being an initial value giving rise to a solution with a different return time  $T$ . Looking for frequency locked solutions corresponds to picking on each branch the solution that has the required value of  $T$ , and ignoring the others, as shown in Figure 16.

**Theorem 14.** If  $\gamma(1 - k_1) < M$ , then there are two frequency locked solutions of (6.16) with period  $n\pi/\omega$ ,  $n \in \mathbf{N}$ , for the following values of  $\omega$ , according to the regions in Proposition 10:

- (2)  $\omega \in (n\pi/T_2, n\pi/T_1)$ ;
- (3)  $\omega \in (n\pi/T_2, n\pi/T_1)$  and  $\omega \in (n\pi/T_4, n\pi/T_3)$ ;
- (5)  $\omega < n\pi/T_2$  and  $\omega > n\pi/T_1$ ;
- (4) all  $\omega > 0$ ;

where the  $T_j$   $j = 1, \dots, 4$  have the values of Proposition 10.

A similar reasoning may be applied to invariant sets for the problem (6.16). When  $T$  is an integer multiple of the forcing period, a  $\mathcal{G}_T$ -invariant set corresponds to a  $G$ -invariant set on the cylinder, that may be lifted to a flow-invariant set for the periodically forced differential equation. We will also say that these sets and their lifts are *frequency locked*. The simplest example are the invariant closed curves arising either in Hopf bifurcations or in homoclinic tangencies, for the problem (6.16). These bifurcation values are denoted  $T_{H_1}$  and  $T_{H_2}$  in the first part of the next result. A more complicated example arises between two homoclinic tangencies, denoted  $T_{h_1}$  and  $T_{h_2}$  in the next corollary, where a transverse homoclinic connection creates chaotic dynamics nearby.

**Theorem 15.** For the values of  $(k_1, \gamma)$  and of  $T \in (T_{H_1}, T_{H_2})$  where there is a closed curve, invariant under the map  $\mathcal{G}_T(s, y)$ , it follows that for  $\omega \in (n\pi/T_{H_2}, n\pi/T_{H_1})$ ,  $n \in \mathbf{N}$ , there is a  $G$ -invariant curve on the cylinder that corresponds to a frequency locked invariant torus for (2.1).

Similarly, when for  $T \in (T_{h_1}, T_{h_2})$  the map  $\mathcal{G}_T(s, y)$  has an invariant set with dynamics conjugate to a shift on a finite number of symbols, then for  $\omega \in (n\pi/T_{h_2}, n\pi/T_{h_1})$ ,  $n \in \mathbf{N}$ , there is a frequency locked suspended horseshoe for (2.1).

The next result shows that there is no gain in looking for different multiples  $n\pi/\omega$ ,  $n \in \mathbf{N}$  of the period, because we obtain essentially the same solution for all  $n$ . To do this, we want to solve:

$$(6.21) \quad G(s, y) = \left( s - \frac{2\alpha}{(\alpha + \beta)^2} \ln y, y^\delta + \gamma(1 + k_1 \sin(2\omega s)) \right) = \left( s + \frac{n\pi}{\omega}, y \right)$$

Solving the first component we get  $y$  as a function of  $\omega \in \mathbf{R}^+$ :

$$(6.22) \quad y(\omega) = e^{\frac{-\widehat{K}n}{\omega}} \quad \text{where} \quad \widehat{K} = \frac{\pi(\alpha + \beta)^2}{2\alpha} > 0.$$

Let

$$F_n(\omega) = e^{\frac{-\widehat{K}n}{\omega}} - e^{\frac{-\delta\widehat{K}n}{\omega}}.$$

In order to find the periodic solutions satisfying (6.16), we need to solve for  $(s, \omega)$  the expression

$$(6.23) \quad F_n(\omega) = \phi_\omega(s) \quad \text{where} \quad \phi_\omega(s) = \gamma(1 + k_1 \sin(2\omega s)).$$

This allows us to relate the frequency locked solutions of (2.1) for different frequencies  $\pi/n\omega$ .

**Proposition 16.** *The pair  $(s_1, \omega_1)$  is a solution of (6.23) for  $n = 1$  if and only if  $(s_n, \omega_n) = \left(\frac{s_1}{n}, n\omega_1\right)$  is a solution of (6.23) for arbitrary  $n$ . This implies that the pair  $(s_1, y)$  is a fixed point of  $G$  in the cylinder, corresponding to a periodic solution of (2.1) with period  $\pi/\omega$  if and only if  $\left(\frac{s_1}{n}, y\right)$  is a fixed point of  $G$  in the cylinder, corresponding to a periodic solution of (2.1) with period  $\pi/n\omega$  for arbitrary  $n \in \mathbf{N}$ .*

*Proof.* That  $(s_1, \omega_1)$  is a solution of (6.23) for  $n = 1$  means

$$F_1(\omega_1) = e^{\frac{-\widehat{K}}{\omega_1}} - e^{\frac{-\delta\widehat{K}}{\omega_1}} = \phi_{\omega_1}(s_1) = \gamma(1 + k_1 \sin(2\omega_1 s_1)).$$

For  $\omega_n = n\omega_1$  we get

$$F_n(\omega_n) = e^{\frac{-\widehat{K}n}{n\omega_1}} - e^{\frac{-\delta\widehat{K}n}{n\omega_1}} = F_1(\omega_1).$$

On the other hand,  $s_n = s_1/n$  yields

$$\phi_{\omega_n}(s_n) = \gamma \left( 1 + k_1 \sin \left( 2n\omega_1 \frac{s_1}{n} \right) \right) = \phi_{\omega_1}(s_1)$$

establishing the claim. Finally,  $y(\omega_n) = e^{\frac{-\widehat{K}n}{n\omega_1}} = y(\omega_1)$ . □

## 7. EQUIVALENCE TO A DISCRETIZATION OF A PENDULUM

In this section, we obtain some additional information on the dynamics of  $G(s, y)$  around a particular type of periodic solution found in Section 6. We do this by an analysis near the middle of the intervals in  $y$  where the periodic solutions may be found. We show that the dynamics around these points is similar to the discretisation of a pendulum with friction and torque.

**7.1. The reduction.** Let  $s_c$  be such that  $\sin(2\omega s_c) = 0$ . If  $\mathcal{G}_T(s_c, y_c) = (s_c, y_c)$  for some  $y_c$ , then it must satisfy  $F(T) = \gamma$  (Figure 17). Hence, a necessary condition for the existence of the solution is  $\gamma \leq M$ . This situation arises in case (3) of Proposition 10 and could also arise in cases (2), (4) and (5). If  $\gamma < M$  then there are two values  $T_*$  for which  $F(T_*) = \gamma$  and for each of these values there are two solutions. Let  $(s_c, y_c)$  denote any of these points, called here *centres of frequency locking*, where  $s_c = n\pi/2\omega$ ,  $n \in \mathbf{N}$  as in Figure 17. Without loss of generality we may take  $n \in \{1, 2\}$ , since we are considering coordinates  $s \pmod{\pi/\omega}$ . These solutions correspond to periodic solutions on the cylinder when  $T_* = \ell\pi/\omega$ ,  $\ell \in \mathbf{N}$ , as discussed in § 6.5 and illustrated in Figure 16. Therefore the centre of frequency locking satisfies  $y_c = e^{-KT_*} = e^{-K\ell\pi/\omega}$ ,  $\ell \in \mathbf{N}$ .

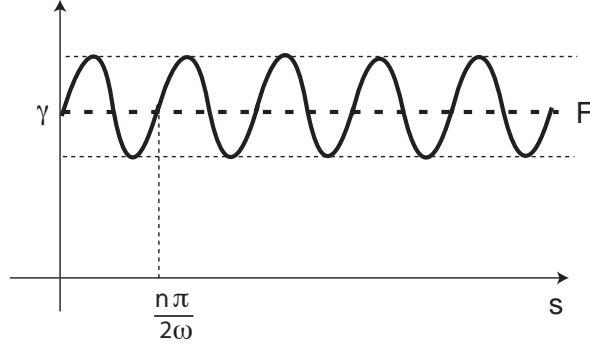


FIGURE 17. Centres of frequency locking.

**Lemma 17.** For each  $\gamma < M$ ,  $\delta \gtrsim 1$  and for  $(s, y)$  there is a centre of frequency locking at  $(s_c, y_c) = (n\pi/2\omega, e^{-K\ell\pi/\omega})$ ,  $\ell \in \mathbf{N}$ ,  $n \in \{1, 2\}$ , provided  $F(\ell\pi/\omega) = \gamma$ . For  $(s, y)$  near  $(s_c, y_c)$  the orbit  $(s_{n+1}, y_{n+1}) = G(s_n, y_n)$  on the cylinder is approximated by the orbit of:

$$\begin{cases} x_{n+1} - x_n = \frac{\gamma}{y_c} (-x_n + k_1 \sin(\theta_n)) \\ \theta_{n+1} - \theta_n = 2\omega \left( \frac{\ell\pi}{\omega} - \frac{x_n}{K} \right) \end{cases}$$

in coordinates  $\theta = 2\omega s$  and  $x = (y/y_c) - 1$ .

*Proof.* By (6.20) and using the definition of  $y_c$ , one knows that:

$$(7.24) \quad y_c = y_c^\delta + \gamma$$

and from (6.16) at  $T_* = \ell\pi/\omega$  it follows that

$$(7.25) \quad \ln y_c = -\frac{\ell K \pi}{\omega} \quad \ell \in \mathbf{N}.$$

We want to analyse the orbit  $(s_{n+1}, y_{n+1}) = G(s_n, y_n)$  with  $s \pmod{\pi/\omega}$ , given by

$$(7.26) \quad y_{n+1} = y_n^\delta + \gamma (1 + k_1 \sin(2\omega s_n))$$

$$(7.27) \quad s_{n+1} = s_n - \frac{\ln y_n}{K} \quad s_{n+1}, s_n \pmod{\pi/\omega}$$

taking  $(s_1, y_1)$  in a neighbourhood of  $(s_c, y_c)$ . In the new coordinates  $(\theta, x) = (2\omega s, (y/y_c) - 1)$  we have that  $y$  near  $y_c$  is replaced by  $x$  near 0. Writing (7.26) in the new coordinates, using  $y = y_c(1+x)$  and (7.24) yields

$$\begin{aligned} y_{n+1} = y_c(1+x_{n+1}) &= y_c^\delta(1+x_n)^\delta + \gamma(1+k_1 \sin(\theta_n)) \\ &\stackrel{(7.24)}{=} (y_c - \gamma)(1 + \delta x_n + O(x_n^2)) + \gamma(1+k_1 \sin(\theta_n)) \quad (\text{expanding } (1+x_n)^\delta) \\ &\approx (y_c - \gamma)(1 + \delta x_n) + O(x_n^2) + \gamma(1+k_1 \sin(\theta_n)) \\ &= (y_c - \gamma)(1+x_n) + (y_c - \gamma)(\delta - 1)x_n + O(x_n^2) + \gamma(1+k_1 \sin(\theta_n)). \end{aligned}$$

Since  $\delta \gtrsim 1$ , we may disregard the terms multiplied by  $(\delta - 1)$ , as well as those  $O(x_n^2)$ , leading to the approximation:

$$\begin{aligned}
 x_{n+1} - x_n &= \frac{y_{n+1}}{y_c} - \frac{y_n}{y_c} \\
 &\approx \frac{(y_c - \gamma)(1 + x_n)}{y_c} - \frac{y_c(1 + x_n)}{y_c} + \frac{\gamma}{y_c}(1 + k_1 \sin(2\omega_n s_n)) \\
 (7.28) \quad &= (1 + x_n) - \frac{\gamma(1 + x_n)}{y_c} - (1 + x_n) + \frac{\gamma}{y_c}(1 + k_1 \sin(2\omega_n s_n)) \\
 &= \frac{-\gamma}{y_c} x_n + \frac{\gamma}{y_c} k_1 \sin(2\omega_n s_n) \\
 &= \frac{\gamma}{y_c} [-x_n + k_1 \sin(2\omega_n s_n)]
 \end{aligned}$$

Using (7.25) in equation (7.27) in the new coordinates we get

$$s_{n+1} = \frac{\theta_{n+1}}{2\omega} = \frac{\theta_n}{2\omega} - \frac{\ln y_c}{K} - \frac{\ln(1 + x_n)}{K} \approx \frac{\theta_n}{2\omega} - \frac{\ell\pi}{\omega} - \frac{x_n}{K} + O(x_n^2)$$

from which we get the approximation

$$(7.29) \quad \theta_{n+1} - \theta_n = 2\omega \left( \frac{\ell\pi}{\omega} - \frac{x_n}{K} \right)$$

as required.  $\square$

**Theorem 18.** For  $\gamma < M$ ,  $\delta \gtrsim 1$  and for  $(s, y)$  near a centre of frequency locking at  $(s_c, y_c) = (n\pi/2\omega, e^{-K\ell\pi/\omega})$ ,  $\ell \in \mathbf{N}$ ,  $n \in \{1, 2\}$ , with  $B(\ell\pi/\omega) = \gamma$ , the dynamics of (4.8) is approximated by the discretisation of the equation for a damped pendulum with constant torque  $\theta'' + A\theta' + \sin \theta = B$  where  $\theta' = d\theta/d\tau$  for  $\tau = \sqrt{2\gamma\omega k_1/K y_c}$ , with  $A = \sqrt{\frac{\gamma K}{2\omega k_1 y_c}} > 0$  and  $B = \frac{K\ell\pi}{\omega k_1} > 0$ .

*Proof.* Consider  $\hat{\tau} = \gamma/y_c$ . From (7.24) it follows that  $\gamma = y_c - y_c^\delta$  and hence using (7.25) we get

$$\hat{\tau} = \frac{\gamma}{y_c} = 1 - y_c^{\delta-1} = 1 - e^{-\frac{K\ell\pi(\delta-1)}{\omega}}.$$

We are interested in the behaviour when  $\hat{\tau} \rightarrow 0$ . Expressions (7.28) and (7.29) may be rewritten as

$$\frac{x_{n+1} - x_n}{\hat{\tau}} = -x_n + k_1 \sin(\theta_n) \quad \text{and} \quad \frac{\theta_{n+1} - \theta_n}{\hat{\tau}} = \frac{2\ell\pi y_c}{\gamma} - \frac{2\omega y_c}{\gamma K} x_n$$

showing that (7.28) and (7.29) may be identified to the discretisation by Euler's method of the following ordinary differential equation with independent variable  $\hat{\tau}$ :

$$\begin{cases} \frac{dx}{d\tau} = -x + k_1 \sin \theta \\ \frac{d\theta}{d\tau} = \zeta - \xi x \end{cases} \quad \text{where} \quad \zeta = \frac{2\ell\pi y_c}{\gamma} \quad \text{and} \quad \xi = \frac{2\omega y_c}{\gamma K}$$

which is equivalent to the autonomous second order differential equation:

$$\theta'' + \theta' + k_1 \xi \sin \theta = \zeta.$$

Rescaling the time as  $\tau = \hat{\tau} \sqrt{k_1 \xi}$ , the previous equation is equivalent to:

$$k_1 \xi \theta'' + \sqrt{k_1 \xi} \theta' + k_1 \xi \sin \theta = \zeta$$

or, equivalently:

$$\theta'' + A\theta' + \sin \theta = B, \quad \text{where} \quad A = \frac{1}{\sqrt{k_1 \xi}} = \sqrt{\frac{\gamma K}{2\omega k_1 y_c}}, \quad \text{and} \quad B = \frac{\zeta}{k_1 \xi} = \frac{K\ell\pi}{\omega k_1}.$$

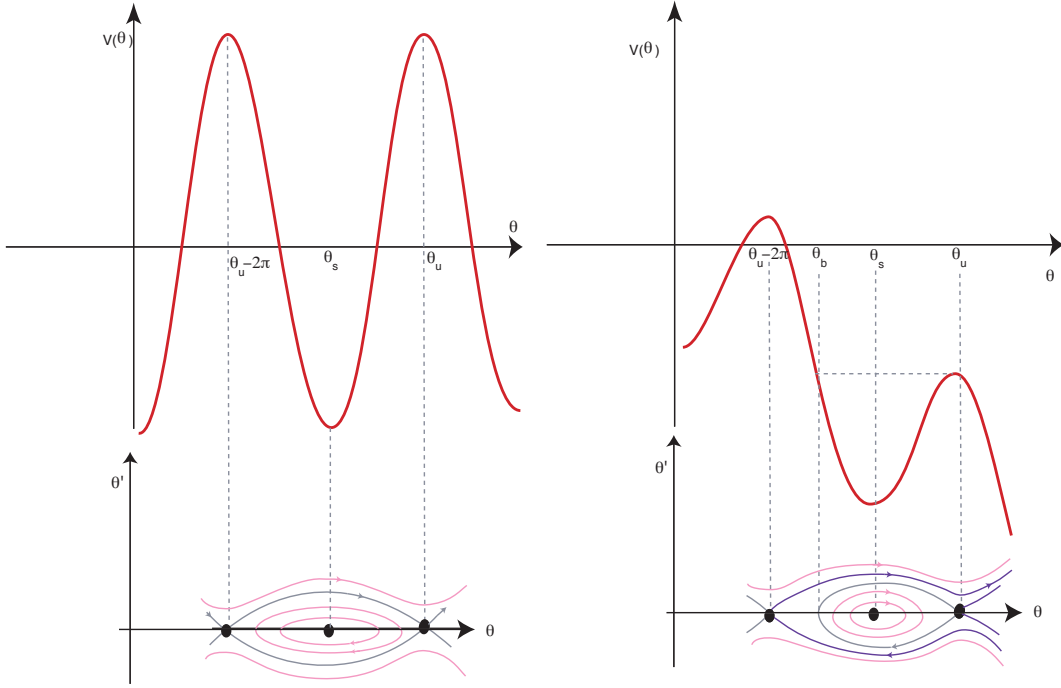


FIGURE 18. Phase portraits for the pendulum with no friction. Left: no torque,  $B = A = 0$ . Right:  $A = 0$  and  $B \neq 0$ .

Finally, note that after rescaling we have:

$$\tau = \frac{\gamma\sqrt{k_1\xi}}{y_c} = \frac{\gamma}{y_c} \sqrt{\frac{2\omega k_1 y_c}{\gamma K}} = \sqrt{\frac{2\omega k_1 \gamma}{K y_c}},$$

as required.  $\square$

Note that from the expression of  $\tau$  after rescaling, we get  $\tau \rightarrow 0$  when either  $\gamma \rightarrow 0$  or  $\omega \rightarrow 0$ .

**7.2. Analysis of the pendulum.** We summarise here the description of the dynamics of the pendulum with torque from [1, Chapter VII] and [11].

In the case  $A = B = 0$ , the equation reduces to that of a simple pendulum with no friction. There is a first integral where the potential is  $V(s) = -\cos s$ . There are two equilibria, a centre at  $\theta_s = 0 \pmod{2\pi}$  and a saddle at  $\theta_u = \pi \pmod{2\pi}$ . There is a pair of solutions connecting the saddle to its copy (see the left hand side of Figure 18), forming two homoclinic cycles. The region delimited by these cycles contains the centre and is foliated by closed orbits with small period, small oscillations of the pendulum. Outside this region there are closed trajectories that go around the cylinder, corresponding to large rotations where the pendulum goes round indefinitely. The small closed orbits are curves homotopic to a point in the cylinder, whereas the large rotations cannot be contracted on the cylinder.

In the case  $A = 0$  and  $B \neq 0$ , the potential is given by  $V(s) = -Bs + \cos s$ , for a pendulum with torque and no friction. If  $B > 1$  there are no equilibria. If  $B < 1$ , the two equilibria  $\theta_s$  and  $\theta_u$  (described above) move but still exist and retain their stability. Let  $\theta_b$  be the value of  $\theta \neq \theta_u$  at which the potential has the value  $V(\theta_u)$ . The solution with initial condition  $(\theta, \theta') = (\theta_b, 0)$  has  $\alpha$ - and  $\omega$ -limit  $\{\theta_u\}$ , so it forms a homoclinic loop, delimiting a region containing  $\theta_s$  and foliated by closed trajectories (see the right hand side of Figure 18). Each one of the other branches of the stable and unstable manifolds of  $\theta_u$  extend indefinitely, forming a helix around the cylinder. Solutions starting

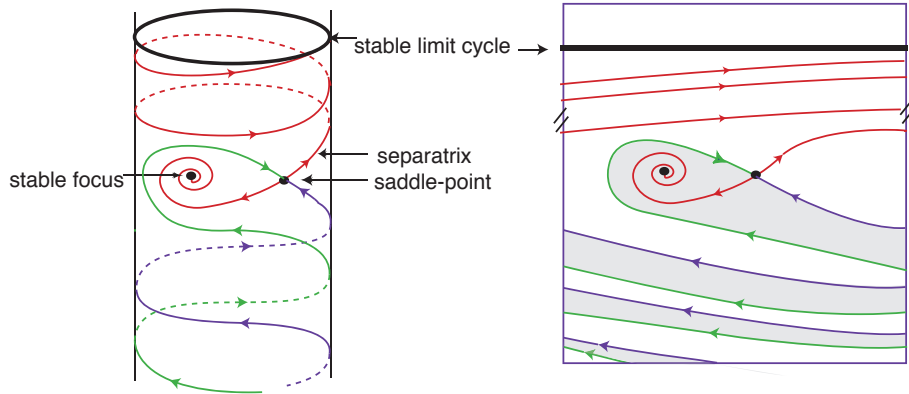


FIGURE 19. Phase portrait for the pendulum with torque, in a region of bistability. Right: the same phase portrait on a chart covering the cylinder. Points in the grey region have the stable focus as  $\omega$ -limit, trajectories of points in the white region go to the stable limit cycle.

outside the homoclinic loop turn around the cylinder infinitely many times both in positive and in negative time.

If  $A \neq 0$  and  $B < 1$ , weak forcing and damping exist. There is a curve in the parameter space  $(B, A)$ , say  $A = \beta(B)$ , that separates two types of dynamics:

- If  $A > \beta(B)$ , then the only stable solution is the equilibrium  $\theta_s$ .
- If  $A < \beta(B)$ , there is bistability (Figure 19): a stable equilibrium and a periodic solution coexist. Depending on the initial condition, the solution should converge either to  $\theta_s$  or to a periodic solution in which the energy lost by damping during one period is balanced by gain in potential energy due to the torque.

Finally, if  $A \neq 0$  and  $B > 1$  there are no equilibria and only one stable periodic solution, that is not homotopic to a point in the cylinder.

## 8. DISCUSSION

We complete our analysis describing the consequences of these results for the map  $G(s, y)$  of (4.8) and specially for the equation (2.1). The dynamical consequences obtained by different methods may coincide in some cases. We use the amplitude  $\gamma > 0$  of the perturbation as a main bifurcation parameter.

For  $\delta \gtrsim 1$  the map  $G(s, y)$  is a good approximation of the first return map for (2.1), while at the same time, near the centre of frequency locking it behaves like the time-one map for the damped pendulum with torque. We start the analysis by the interpretation of the consequences of the data on the pendulum.

Consider  $k_1$  and  $K$  fixed. For each  $\gamma < M$  and each  $\ell \in \mathbf{N}$  there are two values of  $\omega > 0$  such that  $\gamma = F(\ell\pi/\omega)$ . These are the parameter values in Lemma 17 for the existence of the centre of frequency locking. For simplicity we restrict the discussion to the case  $\ell = 1$ , where the centre of frequency locking is a fixed point of  $G$ . Proposition 16 allows us to extend the results to other multiples of the perturbing frequency.

When  $\gamma$  decreases, the largest value of  $\omega$  such that  $F(\pi/\omega) = \gamma$  increases (see Figure 9). Taking  $\gamma$  small enough ensures  $F(\pi/\omega) = \gamma$  with  $\omega > K\pi/k_1$  and this guarantees  $B < 1$  in Theorem 18. This is the case when the approximation by the pendulum equation is reasonable: if  $B > 1$  there is no equilibrium solution for the pendulum, and hence, no frequency locked fixed point.

In Theorem 18, the expression for the pendulum constant  $A$  is a decreasing function of  $\gamma$ , while  $B$  does not depend on  $\gamma$ . The region of bistability occurs for  $A < \beta(B)$  and  $B < 1$ , hence for small enough  $\gamma > 0$ , an attracting fixed point of  $G$  coexists with a closed invariant curve, the graph

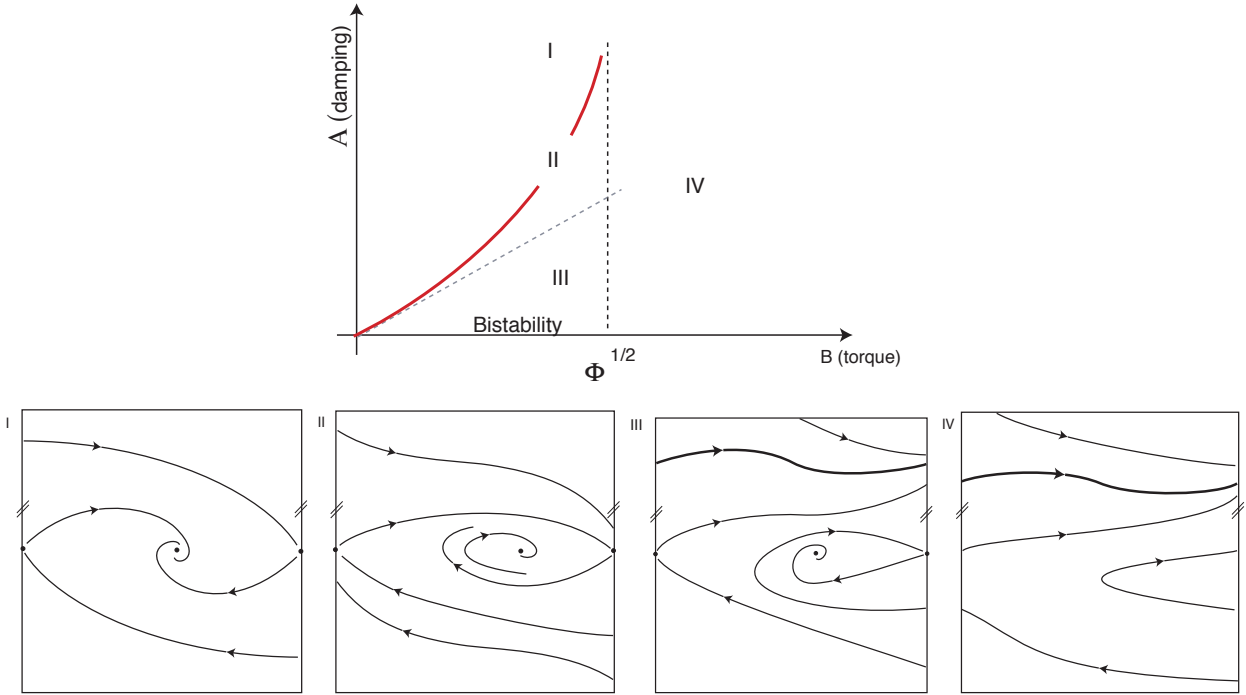


FIGURE 20. Top: bifurcation diagram for the pendulum with torque and corresponding phase portraits below. For parameters on the red curve II there is a homoclinic trajectory connecting two successive copies of the saddle. The thicker curve in regions III and IV is a closed trajectory on the cylinder.

of a function  $y = f(s)$  on the cylinder. This invariant curve probably coincides with the curve obtained in Theorem 7. If this is the case, the attracting fixed point must lie outside the annulus  $|y - \hat{y}| < R\gamma$ , which is not an unreasonable assumption if  $\gamma$  is small. For the equation (2.1) this means there exists an attracting invariant torus in the extended phase space  $\mathbf{R}^3 \times \mathbf{S}^1$  coexisting with an attracting frequency locked periodic solution. When  $\gamma$  increases in this regime, the periodic solution of the pendulum equation disappears at a homoclinic connection. Only the frequency locked periodic solution of (2.1) persists. This is compatible with the hypotheses of Theorem 7, that requires both  $\gamma < M$  and  $\Psi(\hat{y} \pm R\gamma) > Z$ .

The results of Section 6 are more global in that they are valid away from the centre of frequency locking and concern the map  $G(s, y)$  without requiring  $\delta \gtrsim 1$ . This last assumption, however, must be made to extend the results from the map  $G(s, y)$  of (4.8) to the equation (2.1).

If  $k_1 > 1$  and for small  $\gamma > 0$ , Proposition 13 and Theorem 14 guarantee that there exists  $T_2 > 0$  such that for all  $\omega \in (0, \pi/T_2)$  there is an attracting fixed point of  $G$  on the cylinder, as well as a saddle fixed point. The two fixed points come together at a saddle-node for  $\omega = \pi/T_2$ . Another pair of fixed points, a saddle and a source, exist for  $\omega > \pi/T_1$  with  $T_1 < T_2$ , becoming a saddle-node at  $\omega = \pi/T_1$ .

As  $\gamma$  increases, the two saddle-nodes come together at  $\gamma = M/(1+k_1)$ , at a discrete time Bogdanov-Takens bifurcation. For  $\gamma > M/(1+k_1)$ , two fixed points exist for all values of  $\omega > 0$  and one of them undergoes a Hopf bifurcation where a closed invariant curve is created. This curve is homotopic to a point on the cylinder, hence it does not coincide with the curves of Theorem 7 nor of the pendulum. The curve bifurcates into an attracting region where the dynamics is conjugate to a shift, that exists for  $\omega$  in a closed interval. This confirms the numerical findings of [31]. The Hopf bifurcation and the shift dynamics probably also exists for  $\gamma < M/(1+k_1)$ .

The situation is similar for  $k_1 < 1$  and  $0 < \gamma < M/(1+k_1)$ , except that the pairs of fixed points exist for limited intervals  $\omega \in (\pi/T_4, \pi/T_3) \cup (\pi/T_2, \pi/T_1)$  with  $0 < T_j < T_{j+1}$ . Again, at  $\gamma = M/(1+k_1)$  two saddle-nodes coincide at a Bogdanov-Takens bifurcation with  $T_2 = T_3$ , creating a closed invariant curve and, further on, a region of chaotic dynamics. Further increase in  $\gamma$  destroys the chaos and the closed curve, and finally, when  $\gamma = M/(1-k_1)$ , the two remaining saddle-nodes come together at a second Bogdanov-Takens bifurcation, as in Figure 14.

## REFERENCES

- [1] A.A. Andronov, A.A. Vitt, S.E. Khaikin, *Theory of oscillators*, Translation published by Pergamon Press, Oxford, 1966, reprinted by Dover, Mineola, 1987
- [2] V.I. Arnold, V.S. Afraimovich, Y.S. Il'yashenko, L.P. Shil'nikov, *Dynamical Systems V — Bifurcation Theory and Catastrophe Theory* Encyclopaedia of Mathematical Sciences, Springer, 1964
- [3] V.S. Afraimovich, S-B Hsu, H. E. Lin, *Chaotic behavior of three competing species of May Leonard model under small periodic perturbations*. Int. J. Bif. Chaos, 11(2), 435–447, 2001
- [4] V. S. Afraimovich, S. B. Hsu, *Lectures on Chaotic Dynamical Systems*, American Mathematical Society and International Press, 2002
- [5] M.A.D. Aguiar, S.B.S.D. Castro, I.S. Labouriau, *Dynamics near a heteroclinic network*, Nonlinearity 18, 391–414, 2005
- [6] M.A.D. Aguiar, S.B.S.D. Castro, I. S. Labouriau, *Simple Vector Fields with Complex Behavior*, Int. J. Bif. and Chaos, Vol. 16 No. 2, 369–381, 2006
- [7] H. Broer, R. Roussarie, C. Simó, *Invariant circles in the Bogdanov-Takens bifurcation for diffeomorphisms*, Ergod. Th.& Dynam. Sys. 16, 1147–1172, 1996
- [8] M. Cartwright, J. Littlewood, *On nonlinear differential equations of the second order*. J. London Math. Soc. 20, 180–189, 1945
- [9] F. Chen, A. Oksasoglu, Q. Wang, *Heteroclinic tangles in time-periodic equations*, J. Differential Equations, 254 (3), 1137–1171, 2013
- [10] N. Chernov, G. Eyink, J. Lebowitz, Ya. Sinai, *Steady-state electrical conduction in the periodic Lorentz gas*. Commun. Math. Phys. 154, 569–601, 1993
- [11] P. Couillet, J.M. Gilli, N. Monticelli, N. Vandenberghe, *A damped pendulum forced with a constant torque*, American Journal of Physics, 73, 1122–1128, 2005
- [12] J. Dawes, T.-L. Tsai, *Frequency locking and complex dynamics near a periodically forced robust heteroclinic cycle*, Phys. Rev. E, 74 (055201(R)), 2006
- [13] J. Guckenheimer, P. Holmes, *Structurally stable heteroclinic cycles*, Math. Proc. Camb. Phil. Soc., 103, 189–192, 1988
- [14] P. Kloeden, M. Rasmussen, *Nonautonomous dynamical systems*, American Mathematical Society, Mathematical Surveys and Monographs, 176, 2011
- [15] M. Krupa, *Robust heteroclinic cycles*, J. Nonlinear Sci., 7, 129–176, 1997
- [16] M. Krupa, I. Melbourne, *Asymptotic Stability of Heteroclinic Cycles in Systems with Symmetry*, Ergodic Theory and Dynam. Sys., Vol. 15, 121–147, 1995
- [17] M. Krupa, I. Melbourne, *Asymptotic Stability of Heteroclinic Cycles in Systems with Symmetry, II*, Proc. Roy. Soc. Edinburgh, 134A, 1177–1197, 2004
- [18] N. Levinson, *A second order differential equation with singular solutions*, Ann. Math. 50, No. 1, 127–153, 1949
- [19] R. May, W. Leonard, *Nonlinear aspects of competition between three species*, SIAM J. Appl. Math., 29, 243–253, 1975
- [20] K. J. Palmer, *A generalization of Hartman's Linearization Theorem*, J. Math. Anal. Applications, 41, 753–758, 1973
- [21] C. Postlethwaite, J. Dawes, *Regular and irregular cycling near a heteroclinic network*, Nonlinearity, 18, 1477–1509, 2005
- [22] C. Postlethwaite, J. Dawes, *A codimension-two resonant bifurcation from a heteroclinic cycle with complex eigenvalues*, Dynamical Systems: an International Journal, 21, 313–336, 2006
- [23] M. Proctor, C. Jones, *The interaction of two spatially resonant patterns in thermal convection*, J. Fluid Mech., 188, 301–335, 1988
- [24] M.I. Rabinovich, R. Huerta, P. Varona, *Heteroclinic synchronization: Ultra-subharmonic locking*, Phys. Rev. Lett., 96:014101, 2006
- [25] A. A. P. Rodrigues, *Persistent Switching near a Heteroclinic Model for the Geodynamo Problem*, Chaos, Solitons & Fractals, Vol. 47, 73–86, 2013
- [26] A.A.P. Rodrigues, I.S. Labouriau, *Spiralling dynamics near heteroclinic networks*, Physica D, 268, 34–49, 2014
- [27] V. S. Samovol, *Linearization of a system of differential equations in the neighbourhood of a singular point*, Sov. Math. Dokl, Vol. 13, 1255–1959, 1972

- [28] L. Shilnikov, A. Shilnikov, D. Turaev, L. Chua, *Methods of Qualitative Theory in Nonlinear Dynamics 1*, World Scientific Publishing Co., 1998
- [29] L. Shilnikov, A. Shilnikov, D. Turaev, L. Chua, *Methods of Qualitative Theory in Nonlinear Dynamics 2*, World Scientific Publishing Co., 2001
- [30] T.-L. Tsai, J. Dawes, *Dynamics near a periodically forced robust heteroclinic cycle*. J. Physics: Conference Series 286, 012057, 2011
- [31] T.-L. Tsai, J. Dawes, *Dynamic near a periodically-perturbed robust heteroclinic cycle*, Physica D, 262, 14–34, 2013
- [32] Q.D. Wang, A. Oksasoglu, *On the dynamics of certain homoclinic tangles*, J. Differential Equations 250 (2011) 710751
- [33] K. Yagasaki, *Melnikov's method and codimension-two bifurcations in forced oscillations*, J. Differential Equations, 185, 1–24, 2002

## APPENDIX A. NOTATION

We list the main notation for constants and auxiliary functions used in this paper in order of appearance with the reference of the section containing a definition.

Notation	Definition/meaning	Subsection
$\delta$	$\left(\widehat{\delta}\right)^2 = \frac{(\alpha-\beta)^2}{(\alpha+\beta)^2}$	§ 2.1
$\widehat{\delta}$	$\frac{\alpha-\beta}{\alpha+\beta}$	§ 2.1 § 4.2
$K$	$\frac{(\alpha+\beta)^2}{2\alpha}$	§ 2.3 (check)
$f(2\omega\tau)$	$\sin(2\omega\tau)$	§ 4.1
$K_1$	$\int_s^{T_2(0)} e^{-(\alpha+\beta)(\tau-s)} f(2\omega\tau) d\tau$	§ 4.4
$\widehat{k}$	$\frac{\sqrt{A^2+4\omega^2}}{A^2}$ (with $A = \alpha - \beta$ )	§ 4.4
$\bar{k}$	$\frac{(\alpha-\beta)^2 \widehat{k}}{(\alpha-\beta)^2 + 4\omega^2} = \frac{1}{\sqrt{(\alpha-\beta)^2 + 4\omega^2}}$	§ 4.4
$k_1$	$\frac{\bar{k}}{K_1}$	§ 4.4
$M$	$\delta^{\frac{1}{1-\delta}} - \delta^{\frac{\delta}{1-\delta}}$	§ 2.3
$\widehat{y}$ and $\widetilde{y}$	Stable and unstable fixed points of $g_2(y) = y^\delta + \gamma$	§ 2.3 and § 5.1
$R$	$\frac{2k_1}{1 - \delta \widehat{y}^{\delta-1}} > 0$	§ 5.2
$K_*$	$\frac{4\omega\alpha}{(\alpha + \beta)^2}$	§ 5.3
$F(T)$	$e^{-KT} - e^{-\delta KT}$	§ 6.2
$T_M$	$\frac{\ln \delta}{K(\delta - 1)}$	§ 6.2
$(s_c, y_c)$	$\left(\frac{n\pi}{2\omega}, e^{-K\ell\pi/\omega}\right) \quad n \in \{1, 2\}, \quad \ell \in \mathbf{N}$	§ 7.1
$\tau$	$\sqrt{\frac{2\gamma\omega}{Ky_c}}$	§ 7.1